Seasonal icings reveal subsurface water drainage of a Greenland Ice Sheet outlet glacier

Rebecca McCerery[1], Joseph A. Graly[1], Christopher L. Hansen[2], Kate Winter[1], William P. Gilhooly III[3], Trinity L. Hamilton[2,4], Moses Jatta[3], Jeff R. Havig[2], Felipe Napoleoni[1,5], Alicia M. Rutledge[6], Matthew Terrell[3], Tanya M. Trott[7], Kayla Woodie[3], Bernd Kulessa[7], Sevi Modestou[1], Hannah Bahrani[1], Tori Kennedy[3], Alexandra Messerli[8], Kathy Licht[3]

~~[1]School of Geography and Natural Sciences, Northumbria University, Newcastle upon Tyne, United Kingdom, NE1 8ST~~

*Corresponding author ~~rebecca~~becky.mccerery@manchester.ac.uk~~hotmail.com~~

[1]School of Geography and Natural Sciences, Northumbria University, Newcastle Upon Tyne, NE1 8ST, United Kingdom

[2]Department of Plant and Microbial Biology, University of Minnesota, Saint Paul, MN 55108 USA

[3]Department of Earth & Environmental Sciences, Indiana University Indianapolis, Indianapolis, IN 46202 USA

[4]The BioTechnology Institute, University of Minnesota, Saint Paul, MN 55108 USA

[5]School of Geosciences, University of Edinburgh, Edinburgh, EH8 9XP, United Kingdom

[6]Department of Astronomy and Planetary Science, Northern Arizona University, Flagstaff, AZ 86011 USA

[7]School of Biosciences, Geography and Physics, Swansea University, Swansea, SA2 8PP, United Kingdom

[8]Asiaq Greenland Survey: Nuuk, GL

Abstract

In many glacial settings, winter outflows of proglacial water create stratified domed ice structures on glacial forefields. These structures, called naledi, provide an opportunity to characterise ~~the~~ solute ~~fluxes~~ concentrations ~~of hydrological systems in winter which are poorly constrained compared to summer outflows~~ in hydrological systems during winter, which are poorly constrained compared with summer outflows ~~which are~~ dominated by supraglacial meltwater ~~input~~. To characterise the different hydrological systems feeding naledi and provide conceptual models of their formation, we sampled 12 overwinter naledi and 4 ~~supercooled~~ summer ice accumulations (accreted ice) from the forefield of Isunnguata Sermia, a western outlet glacier of the Greenland Ice Sheet, during four field campaigns. Major ions and stable water isotopes reveal complex geochemical signatures, where the composition of successive naled layers ~~reveal~~ indicates fluctuations in water source and transport throughout winter. In comparison, ~~core analysis of~~ summer accreted ice is sediment laden and shows uniform geochemistry throughout, suggesting freeze-on of water from ~~one~~ a single source in quick, discrete events. These findings are supported by Electrical Resistivity Tomography (ERT) geophysical surveys~~, which reveal~~ showing shallow hydrological pathways (1 – 5 m below the surface) in the glacial foreland (surveyed 400 m from the glacier terminus). ~~Here,~~These ~~meltwater is transported through a saturated sediment zone feeding proglacial upwellings. Our~~ results inform the first conceptual models of summer vs. wintertime subglacial water routing and naled formation in the proglacial zone of the Greenland Ice Sheet. We show that wintertime naledi form from a combination of top-down (unconfined) and bottom-up (confined) freezing processes ~~which incorporates~~incorporating subglacial discharge, overland flow and precipitation~~.~~, In contrast, ~~whereas~~ accreted ice forms from upwellings of ~~high velocity~~high-velocity, ~~highly pressurised~~highly pressurised water which freezes upon release. These seasonal changes drive different geochemical and ~~nutrient~~ solute outputs, which are critical for

evaluating glacier meltwater contributions to proglacial groundwater systems and the impact of glacial discharge on downstream ecosystems.

1. Introduction

The Greenland Ice Sheet is a major exporter of biologically important elements to the world's oceans (Hawkings et al., 2016; Lawson et al., 2014; Wadham et al., 2016) and a hotspot for CO_2 drawdown through chemical weathering processes (Graly et al., 2017a; Pain et al., 2021). Most of our knowledge of chemical and biological fluxes from the Greenland Ice Sheet ~~come~~ comes from analysis of the summer ablation season outflow, where channelised melt waters contact only a limited portion of the glacier bed (Bhatia et al., 2013; Hawkings et al., 2016; Jacob et al., 2014; Meire et al., 2016; Yde et al., 2014). However, during winter, outflow is ~~more~~ typically fed by slower-flowing subglacial meltwater, which has often been subjected to greater contact time with the ice/bed interface (Chandler et al., 2013; Davison et al., 2019). As there are inherent challenges associated with field sampling subglacial water flow over winter, there is limited inclusion of winter water in geochemical modelling, inhibiting our understanding of year-round subglacial weathering processes and nutrient export from Greenland.

In many proglacial environments in the Arctic, domed ice structures called naledi (singular ~~*naled*, but~~*naled* but also referred to as *aufeis* or *icings*) develop within glacier forefields in the winter months (Carey, 1973; Hodgkins et al., 2004; Mallinson et al., 2019; Morse and Wolfe, 2015; Sobota, 2016; Yoshikawa et al., 2007). These naledi typically consist of stratified layers of frozen subsurface and subglacial water ~~that has been d~~discharged over winter (November - March). As such, they provide a potential source for characterising wintertime solute ~~fluxes~~ concentrations and insights into chemical weathering processes operating over low-flow hydrological conditions that are difficult to obtain by other means. Layers build up over winter to produce a domed, layered, ice structure, which can reach multi-

metre heights, forming where outflows of water are expelled in discrete locations of the glacial foreland and quickly freeze due to low air temperatures (Harden et al., 1977; Kane, 1981).

The prevailing theoretical models of naled formation, established ~40 years ago, suggest that naled grow in a top-down fashion because the cold winter atmosphere acts as a heat sink, freezing unconfined waters ~~(meltwater or snow)~~ that accumulate from above (Fig. 1a-c) (Schohl and Ettema, 1986; Yde et al., 2012). However, more recent and direct observations of proglacial naled in Svalbard by Stachnik et al. (2016) interpreted naled formation as a primarily bottom-up process. This theory suggests new meltwaters confined below ice push up older, frozen layers (Fig. 1d-f), and that liquid water conduits within naled ice provide insulated transport pathways, protected from the cold surface (Fig. 1f). These contrasting models of formation make it challenging to extrapolate general chemical and biological insights into different hydrological systems.

In previous research, principally on Svalbard, the chemistry preserved in naled ice has been successfully characterised by analysing ice cores collected in early spring (Stachnik et al., 2016; Wadham et al., 2000; Yde et al., 2012). These studies found that the overwinter solute flux captured in naled ~~differ~~ differs significantly from the early spring or late summer meltwater output from glacial systems, suggesting they can capture a distinct wintertime hydrochemical regime (Graly et al., 2018). However, complexity in their geochemistry indicates multiple water source inputs may build up a single naled (Yde et al., 2012) with chemical differences between different ice layers (Stachnik et al., 2016). The glaciers of Svalbard represent relatively small glacier hydrologic systems, with small storage capacities compared to larger ice sheets, like the Greenland Ice Sheet and its outlet glaciers (Wadham et al., 2000). It is therefore possible that the chemical signatures of naled ice in these larger systems may represent different formation mechanisms than those in Svalbard. In glacial foreland areas, supercooled waters can also freeze and build up accreted ice structures over

summer, often during high discharge events sourced from glacial ~~overdeepenings~~overdeepenings that are heavily sediment-laden (Alley et al., 1998; Evenson et al., 1999; Lawson et al., 1998; Roberts et al., 2001; Roberts et al., 2002; Livingstone et al., 2026).

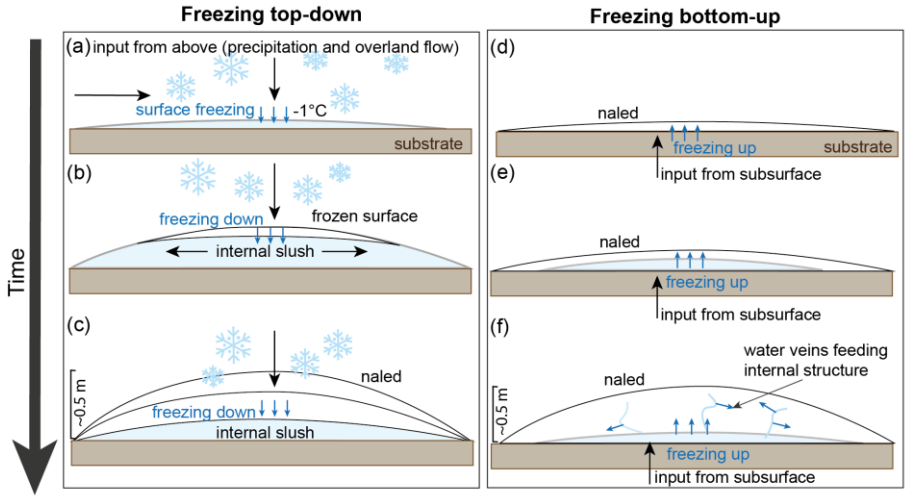


Figure 1 Prevailing theories of naled ice formation. (a-c) A top-down freezing process by which overland flow and precipitation freeze at the surface due to subzero air temperatures (Schohl and Ettema, 1986). (d-f) A bottom-up freezing process by which subsurface waters erupt into the forefield and freeze from the base-up, with newly erupting waters accreting onto the bottom of the naled. In these bottom-up models, there is also potential for small water veins within the naled to accrete ice within (Wadham et al., 2000; Stachnik et al., 2016).

Here, we measure and interpret the chemical characteristics and identify the sources of water creating wintertime naled ice and summertime accreted ice in the forefield of Isunnguata Sermia on the western Greenland Ice Sheet~~, .~~ ~~to explore seasonal changes in the hydrological system.~~ We combine our geochemical analyses with geophysical surveys of the forefield to assess potential routing mechanisms of water flow~~,~~ feeding these structures and explore seasonal changes in the hydrological system. Our results inform a new conceptual model of naled and accreted ice formation ~~and has~~applicable ~~applications for spatial and temporal~~

~~analysis of~~to similar proglacial systems ~~and subglacial processes~~ in West Greenland and other glaciated regions.

2. Study site

Isunnguata Sermia (N67.1850, W-50.3394) drains ~15,900 km^2 of the Greenland Ice Sheet and is located approximately 100 km away from the coast (Fig. 2) (Lindbäck et al., 2015). ~~It~~ The outlet glacier is located in the central west region of Greenland, ~~where ice is~~ routed through an overdeepened bed (extending to ~350 m below sea level) for over 20 km (Lindbäck et al., 2015). Throughout its catchment area, Isunnguata Sermia is expected to flow over granodioritic gneisses and associated silicate rocks of the Nassuttooqidian Orogen, a large-scale fold-belt formed c. 2.7 billion years ago (van Gool et al., 2002).

Previous work has characterised spring/summer runoff and subglacial hydrology at Isunnguata Sermia (Bartholomew et al., 2011; Meierbachtol et al., 2013) as well as subglacial discharge and hydrochemistry of summer outflows (Graly et al., 2017a). Wintertime outflow was chemically profiled by Pitcher et al. (2020), who sampled proglacial river water while performing local radar surveys of Isunnguata Sermia. This revealed that basal water is persistent at Isunnguata Sermia, discharging small amounts of water into the proglacial river system year-round. Isunnguata Sermia also sits on a reverse gradient bed slope with an active subglacial lake system (Livingstone et al., 2019). These lakes, located beneath the ablation zone of Isunnguata Sermia, have been shown to exhibit multi-year water storage, resulting in long water residence times, though research has also shown that meltwater can be quickly released during flood events (Chu et al., 2016; Livingstone et al., 2019).

The forefield of Isunnguata Sermia contains several ~~discreet~~ discrete upwellings of subglacial water. These waters may emerge slowly, or as geyser-like features that expel water into the air on a ~~meter~~ metre- to multi-~~meter~~ metre scale (Livingstone et al., 2026). In February 2015, supercooled water was discovered below the clear ice of a proglacial outlet stream, 1 km

downstream of the Isunnguata Sermia terminus (Pitcher et al., 2020). This slow meltwater drainage, fed by the deeply incised subglacial trough that extends inland from the terminus (Graly et al., 2017a), suggests that the local geometry might drive proglacial upwellings of subglacial meltwater year-round. As a result, this site provides an ideal location to investigate the geochemical signature of water sources feeding naled ice and accreted ice, allowing us to examine changes in hydrological pathways and fully characterise the chemical signature of year-round outflows, for the first time.

3. Methods

3.1. Automatic cameras

Monitoring of glacier outflow and the development of naledi ~~were~~ was ~~performed~~done by setting up ~~timelapse~~ time-lapse cameras (LTL-6210MC Plus Scouting Cameras) ~~at six locations~~ across the glacier forefield ~~over winter in 2022 and 2023~~and monitored between 2022 and 2024 (Fig. 2 and Table SI1). Cameras were set up at ~~various~~ six different locations and orientations to capture changes in the main outflow channel of Isunnguata Sermia and to review active upwellings at the time of installation. Photographs were taken at ~~11am~~11 am, ~~12pm~~12 pm, ~~1pm~~ 1 pm and ~~2pm~~ 2 pm (local time) each day. Full descriptions of camera installations and observations can be found in Supplementary Information Table SI1.

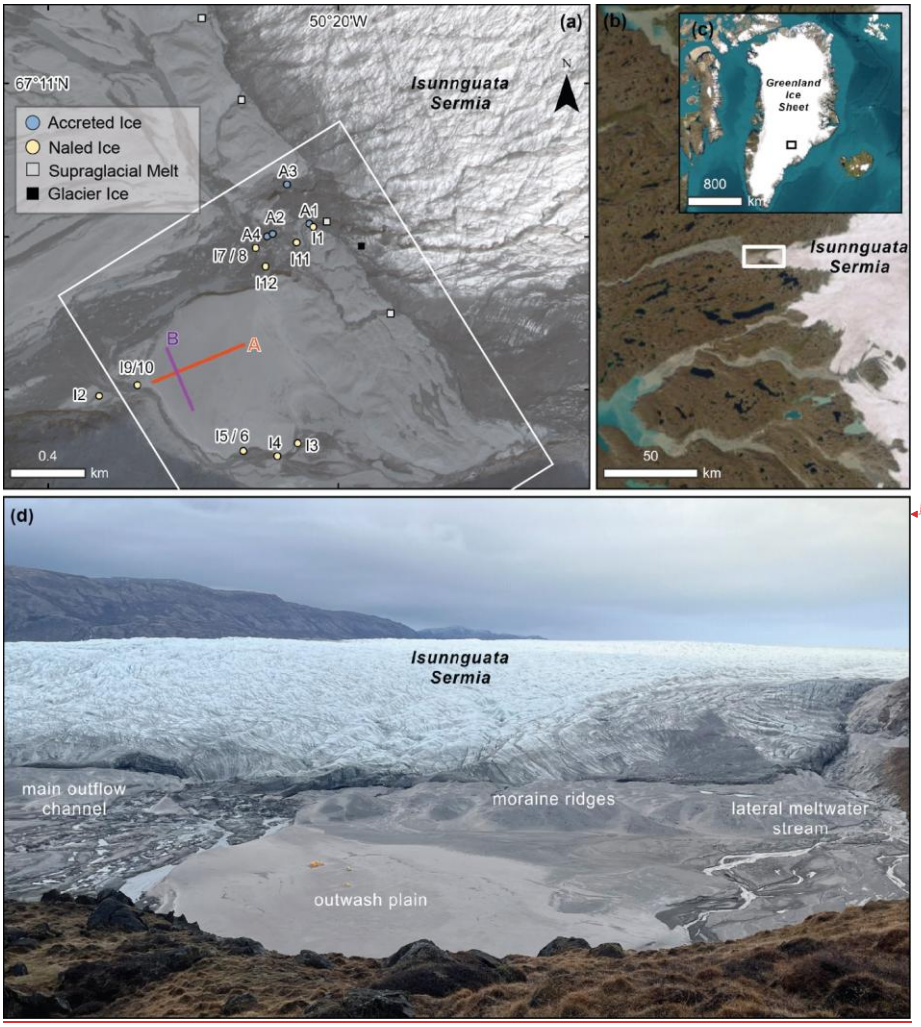
3.2. Sampling

Four field campaigns were conducted ~~with the aim of collecting~~to collect a representative sample set of ice and water samples across the Isunnguata Sermia forefield over multiple years both pre- and post-melt season (Fig. 2). We focused on three different sample types (i) naled ice (dome shaped structures, formed over winter likely during low discharge), (ii) naled waters upwelling in the outwash plain (capturing active water sources feeding naled ice over the winter

months) and (iii) accreted ice (sediment-laden ice structures associated with active upwellings in the summer months) (Fig. 2).

Over the course of four field campaigns (October 2022, ~~March~~ April 2023, September 2023 and March-April 2024), we sampled 12 naledi and ~~four~~ 4 accreted ice structures (Fig 2a, Fig. S1-2). Ice cores were extracted with a motorised SIPRE Auger to a maximum depth of 2 m. Cores were logged immediately, then sectioned by changes in ice facies and transported in individual sterile Whirl-Pak bags (Fig. 3). Core sections were then melted in a gently heated water bath in the field (less than 4 hours after sampling)~~. The resultant waters were~~ and filtered using Whatman 0.45µm cellulose membrane filters~~, before being decanted~~ -into~~to~~ centrifuge tubes for major ion analysis. All samples were refrigerated and stored at 3-4°C until analysis. Four of the naled ice cores terminated in water sources. Cores at the other seven sites did not reach water and were limited to depths ~~of~~ between 8 and 139 cm, often due to ~~the presence of~~ thick gravel ~~beds,~~deposits which rendered further drilling impossible.

Of the cores that reached active water sources, naled I8 was located at the margin of the main meltwater channel and the three others (I2, I3 and I10) in an adjacent lateral meltwater stream (Fig. 2). In each case, samples of the naled upwelling waters were collected in sterile 50 ~~ml~~ mL centrifuge tubes and filtered using Whatman 0.45 µm nylon membrane filters. Accreted ice cores were sampled around the glacier front and within the main active frozen meltwater channel area in October 2022 (n = 4, Fig. 2a, Fig. 4 and Fig. S3). Unlike the naled ice core sites, none of the accreted ice cores reached free-flowing waters. ~~Cores were described, sectioned, melted and filtered in the same manner as described above.~~



187

Formatted: Indent: First line: 0 cm

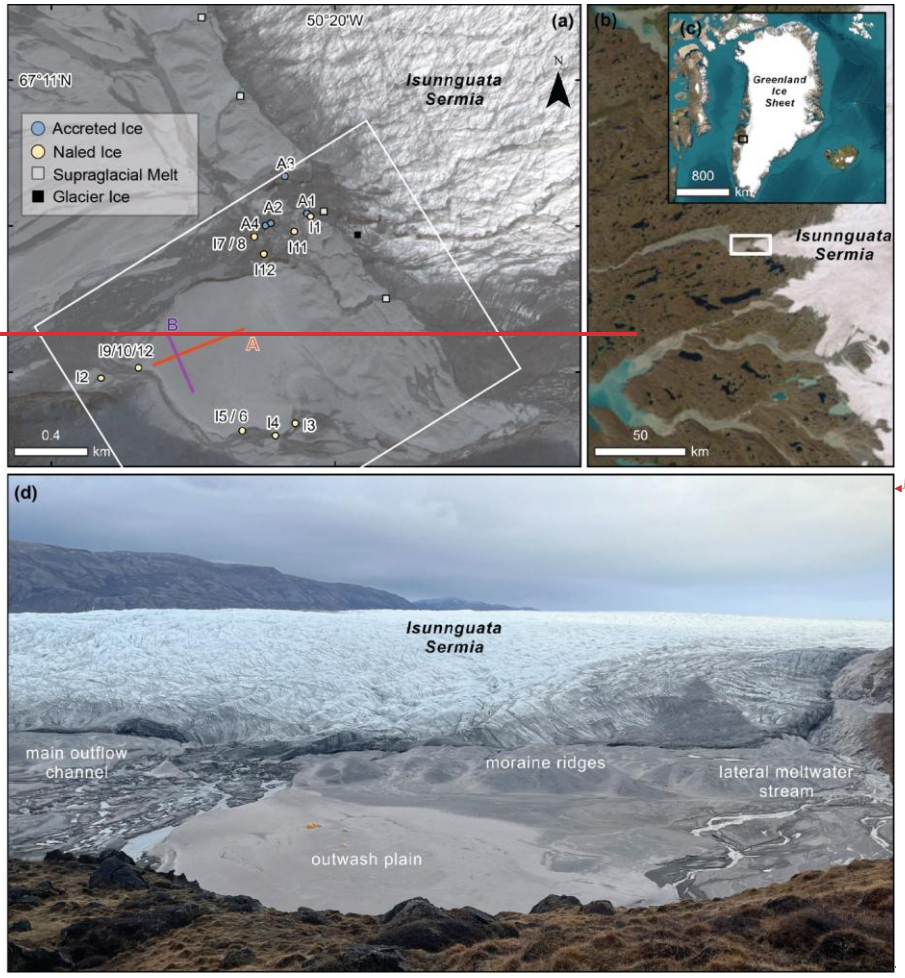


Figure 2. Isunnguata ~~Semia~~ Sermia field site in West Greenland (a) Location of sampling sites, geophysical survey transects (A and B) and camera trap locations in the forefield of Isunnguata Sermia. White box denotes the photograph area shown in (d). (b) Sample area of the Isunnguata Sermia forefield (white box), where meltwater is exported from the Greenland Ice Sheet (c). (d) Overview photograph of the proglacial forefield from May 2023 with key sites annotated. The yellow features on the outwash plain are camp tents, ~~which are~~ approximately 1.6~~ to~~ 1.9 ~~meter~~ms high. Imagery © [2024] Vantor in panel (a) sourced from the Polar Geospatial Centre (showing June 2022) whilst panels b-c show Esri basemap imagery | Powered by Esri. ~~Satellite images in panel a sourced from the Polar Geospatial Centre (from June 2022) and panels b-c Sources: Esri basemap imagery | Powered by Esri.~~

Formatted: Left

Formatted: Font: Not Italic

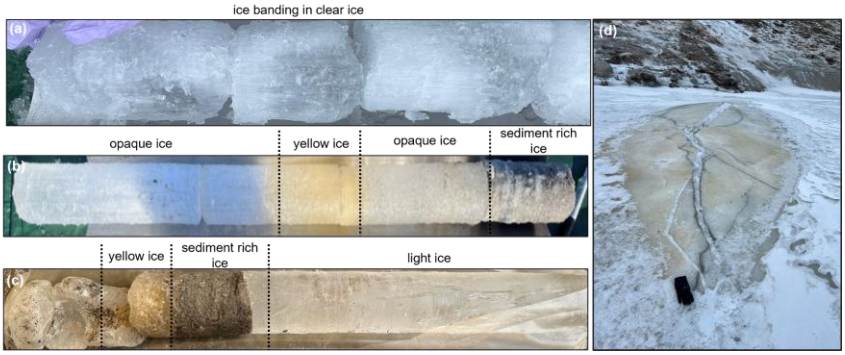


Figure 3 Naled ice structures~~. E~~ and examples of different ice facies from cores~~, drilled through naled ice structures~~ (a) Ce~~ore I3 (15 cm)~~, (b) upper 90 cm of core I10 and (c) lower 68 cm of core I10, as well as a photograph of a naled structure (cored for I10) (d) where a black glove (~20 cm in length) is provided for scale.

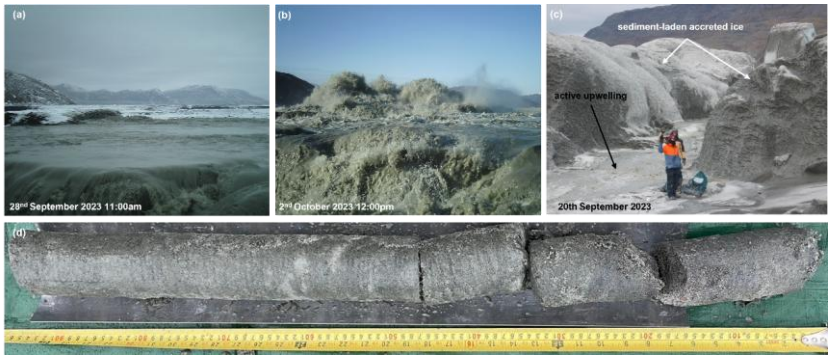


Figure 4 (a-b) Examples of a subglacial water outburst from Isunnguata Sermia, captured by automatic camera 4 in late September to early October 2023. Photographs show high water flow volumes on the 28th of September (a) followed by an erupting outflow 4 days later (b). (c) Example of a multi-metre high accreted ice structure, alongside an active, bubbling upwelling of water, reviewed by field researchers on the 20th of September 2023. (d) Example of a sediment-rich core from an accreted ice structure.

~~**Figure 4** (a-b) Examples of a subglacial water outburst from Isunnguata Sermia, captured by automatic camera 4 in late September to early October 2023. High water flow volumes on the 28th of September (a) were followed by erupting outflow just 4 days later (b). (c) Example of a multi-metre scale accreted ice structure, captures on the 20th of September 2023, showing an active, bubbling upwelling of water in the forefield of Isunnguata Sermia, where accreted ice (~2 m high) has built up to the sides of the upwelling. (d) Example of an ice core from an accreted ice structure, rich in sediment.~~

C~~ontextual~~ontextual samples of glacier ice (n = ~~1~~2) and supraglacial meltwater (n = 47) were also collected to represent ~~end member~~end-member water types. Glacier ice was sampled from the upper ice margin of Isunnguata Sermia in April 2024 using a chisel and hammer, with the upper 10 cm layer of ice discarded to remove the outer layer of weathered ice (Fig. 2a). ~~Ice was extracted via a chisel and hammer with the upper 10 cm layer of ice discarded so that less weathered ice could be sampled.~~ Supraglacial water was sampled from the ice margin and atop the Isunnguata Sermia glacier snout in 50 ~~ml~~mL centrifuge tubes.

3.3. Geochemistry

Concentrations of major anions in water and melted ice samples were analysed in triplicate on a Dionex Integrion high-pressure ion chromatography (~~HP~~IC) system at Northumbria University using 5 ~~ml~~ mL of sample. Standard solutions of fluoride (F^-), chloride (Cl^-), sulphate (SO_4^{2-}), and nitrate (NO_3^-) were prepared using 18.2 MΩ ultrapure water to obtain standard curves. Concentrations of major cations were analysed in triplicate on an Optima 8000 inductively coupled plasma optical emission ~~spectrometer~~spectrometer (ICP-OES) at Northumbria University using 7 ~~ml~~ mL of sample. Standard solutions of calcium (Ca), potassium (K), magnesium (Mg), and sodium (Na) were prepared using ultrapure water to obtain standard curves. Limits of detection (LOD) for both instruments was determined by standard regression on the intercept of the calibration curve and measured 0.02 mg L^{-1}. Analytical precision was assessed as the relative standard deviation (RSD %) of triplicate measurements for each sample. RSD was below 3% for all analytes and across all run days for

Formatted: Line spacing: Multiple 1.15 li

Formatted: Superscript

the ICP-OES and the IC, indicating good analytical reproducibility. HCO_3^- was then calculated using the charge balance error (CBE) method~~,~~, ~~determined by Equation 1~~ where ε^+ and ε^- are total cation and anion equivalents~~:~~. Uncertainty in HCO_3^- concentrations is derived from uncertainties of all measured cation and anion concentrations.

~~$$CBE = \frac{(\varepsilon^+ - \varepsilon^-)}{(\varepsilon^+ + \varepsilon^-)} x100$$~~

~~(Eq. 1)~~

3.4. Stable water isotopes

Aliquots ~~from melted cores and water~~of samples were analysed for their hydrogen and oxygen isotopic composition using a Picarro L2130-i cavity ringdown ~~spectrometer~~spectrometer at Northumbria University. Four calibration standards were measured at the beginning of each run (including in-house laboratory standards supplied and calibrated by the University of Bergen ('EVAP-2', 'FINSE', 'GLW') and international standard SLAP2 (Standard Light Antarctic Precipitation 2). Separate aliquots of reference water 'Medium Natural Water ' or 'Greenland Water' (purchased from Elemental Microanalysis Ltd.) were ~~interspersed~~ analysed ~~approximately~~ every 10~~-~~ to 15 samples ~~tand used t~~o monitor and correct instrument drift. Results were corrected for memory and drift and normalised to the VSMOW-SLAP (Vienna Standard Mean Ocean Water – Standard Light Antarctic Precipitation) scale, using the FARLAB Liquid Water Isotope Measurement Processor (FLIIMP) software package (Sodemann et al., 2023). No humidity correction was applied (following Weng et al., 2020). The drift standards (as well as one aliquot of VSMOW2 per run) were ~~also~~ used as data quality monitors. Analytical error is equal to or better than 0.4‰ for δD and 0.07‰ for $\delta^{18}O$ (SE); overall reproducibility based on monitor standards is equal to or better than 1.0‰ for δD, and 0.38‰ ~~on~~ for $\delta^{18}O$ (SD) (Table SI2). Individual 'freezing ~~packages'~~ packages', which are discrete isotopic units within the naled ice body representing a temporally distinct episode of

water upwelling and subsequent freezing at the ice surface, were also identified by calculating ~~freezing curves~~freezing curves for each ice core. In the context of refreezing Greenland Ice Sheet waters, a δD:$\delta^{18}O$ slope of around 6 ~~is~~ would be expected. The composition of the source water can be calculated from the two-isotope slope (Souchez and Jouzel, 1984), allowing us to determine the isotopic composition of the source water where a freezing slope is identified.

3.5. Electrical Resistivity Tomography

A SuperSting R8 eight-channel earth resistivity ~~meter~~metre (Advanced Geosciences, Inc.)~~,~~ was used to investigate subsurface conditions and potential water transport routes through the forefield of Isunnguata Sermia (Fig. 2) in April 2024. ~~Prior to deployment, t~~The frozen ground had to be prepared for electrode stake deployment~~. For each stake,~~ by ~~small areas of frozen ground were thawed~~thawing small areas to a depth of ~30 cm using boiled water, heated from locally sourced snowmelt. A mixture of locally sourced glacial clay and salt or isotonic powder (Gatorade™) was poured over the thawed ground to secure each electrode stake and ensure sufficient ground coupling once the electrodes froze in. Fifty-six electrodes were installed in a forward and reverse dipole-dipole configuration along profile A with the same configuration along profile B (Fig. 2)~~, where~~ for 47 electrodes~~ were placed~~. The maximum source current was set to 50 mA for both profiles, and electrode contact resistance was monitored throughout. All data ~~were~~ were processed and inverted using ResIPy v3.6.3 (Blanchy et al., 2020)~~. The full data processing methodology is available in the~~ (see Supplementary Information).

4. Results

4.1. Automatic cameras and Field Photos

~~The automatic cameras were set up with the aim of recording the development of naled ice (full descriptions of camera traps and observations can be found in Supplementary Information~~

~~Table SI1).~~ Automatic c~~C~~ameras captured active naled and accreted ice formation as well as~~as well as~~ changes in winter outflow over the foreland of Isunnguata Sermia from 2022 to 2024. In 2023, Camera 5, orientated on the proglacial outwash plain facing the ice margin, ~~for example,~~ captured the formation of winter-accumulating naled ice and an outflow of yellow-coloured water on the 22nd of October ~~2023~~ when the rest of the meltwater channel was frozen (~~shown in~~ Fig. 5). The ~~origins of this yellow water flow are not fully clear and~~source of flow from this yellow water ~~may~~ originate from a location off-camera~~ or from the rising domed naled structure. ; but i~~The~~ts~~ distinct colouration of this water ~~dominated~~ can be seen freezing over the channel and naled structure ~~for~~ over 3 days~~ 3 days~~, ~~where layers of yellow coloured ice seemed to build up from the margins of the outflow,~~ before being covered by fresh snow on 28th October. ~~This created a clear ice layer on top of the yellow covered ice.~~ These accumulation patterns~~, recorded for the first time by our automatic cameras~~ suggest that similar ice layering may be expected in the naled ~~formations~~icings~~, and the ice cores extracted from them~~. ~~This camera also captured the formation of winter accumulating naled ice in the distance (Fig 5).~~

A glacial outburst flood from Isunnguata Sermia was also detected between September and early October 2023 (see Livingstone et al. 2026). By analysing footage from two separate automatic cameras~~, placed in different locations, facing different~~ and orientations (see Supplementary Information), ~~we can see~~ a gradual increase in water levels of the main meltwater channel was observed~~,~~ before a vigorous outburst flood event ~~occurred~~ on October 2nd (Fig. 4a-b)~~.~~. We also observed the sudden build-up of sediment-laden accreted ice around the upwelling during the outburst event (Fig. 6). Much of the resulting accreted ice structure persisted up to 6 months later, preserved by the cold winter temperatures, though it appeared to have eroded, suggesting some melt wastage had occurred.

Formatted: Not Superscript/ Subscript

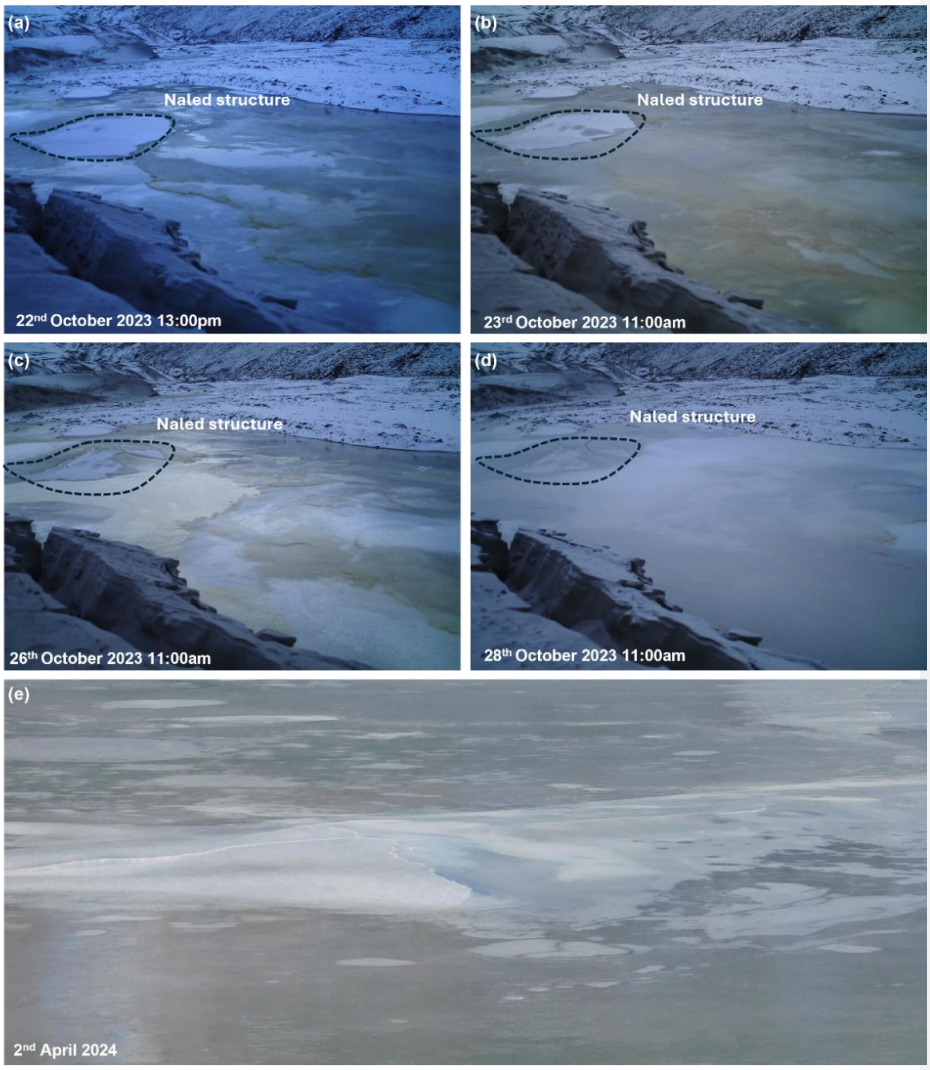


Figure 5 Upwelling of glacial waters in the forefield of Isunnguata Sermia, captured by an automatic camera installation (Camera 5) ~~installed~~ for the 2023/2024 winter season (a-d). Over the course of 6 days, distinctly yellow-coloured water flows and ice accumulations were recorded, suggesting variable water/snow inputs/throughputs. (a) Photograph showing the first emergence of yellow-coloured water in the glacial foreland. (b) The yellow outflow completely covers the proglacial river in the field of view. (c) White ice and snow begin to overlay the

yellow layer, which ~~have~~ has frozen. (d) The yellow ice layer is fully covered with fresh white ice and snow. Black dashed outline highlights the naled ice area. (e) A naled dome formed in the centre of the proglacial stream overnight on the 2nd April 2024, captured in field photographs.

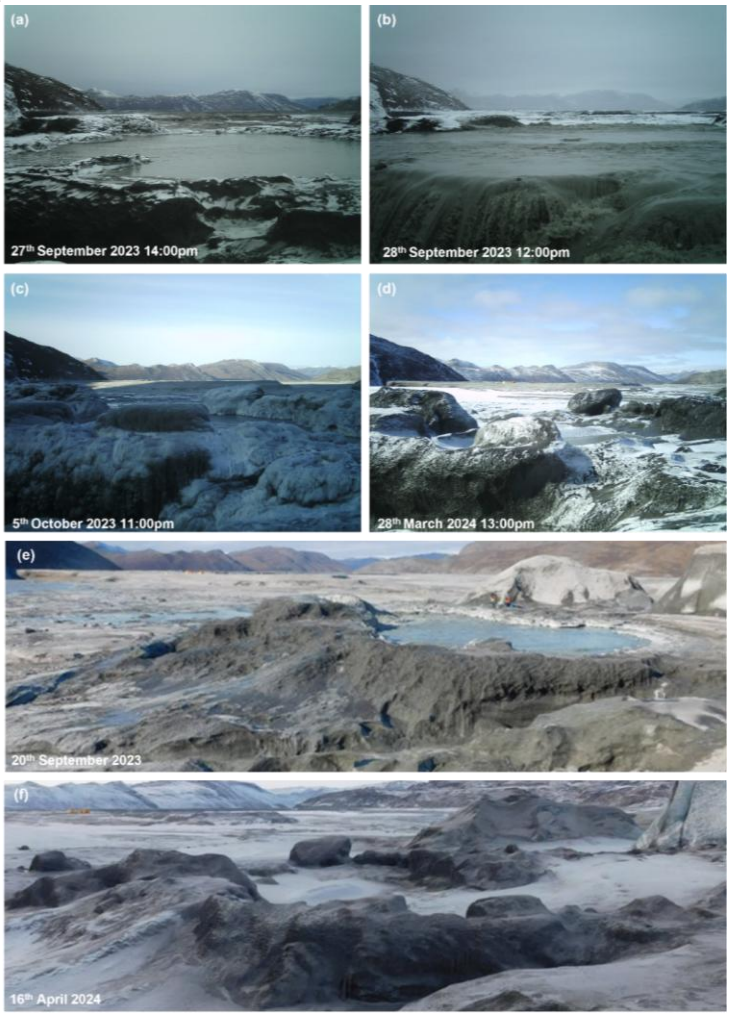


Figure 6 Accreted ice formation (a-d) captured by an automatic camera installation ~~installed~~ for the 2023/2024 winter season. (a-b) Over the course of a week ~~towards the end of the melt season,~~ an eruption of glacial meltwater occurred in the main proglacial meltwater channel close to the Isunnguata Sermia ice margin (Livingstone et al., 2026), see ~~-~~ https://vimeo.com/manage/videos/1103612163. (c) This resulted in the rapid accumulation of ice accretions around the ~~source of the~~ upwelling. (d) Over 6 months later, some ~~of that~~ ice ~~accumulation~~ persists around the upwelling source, ~~likely~~ preserved by the cold winter

temperatures, though the ice structure appears deflated and eroded ~~suggesting some melt wastage has begun to occur~~. A similar process is seen in (e), where sediment-rich ice accumulations around an upwelling site in late September 2023 had deflated and eroded substantially (f) the following April 2024.

4.2. Ice facies analysis

Ice cores revealed distinct ice facies, which we group into four classifications: light ice, opaque ice, yellow-coloured ice, and sediment-rich ice (Fig. 3). Some ice has either horizontal or vertical stripes – which are more visible in the 'light ice' and 'opaque ice'. Light ice and opaque ice packages do not have sediment inclusions or discolouration~~. I~~, with the light ice ~~was~~ mostly translucent~~, whereas~~ and the opaque ~~ice appeared~~ white or '~~clouded~~'clouded ', and ~~, both ice types~~ were combined ~~together~~ for geochemical analysis as 'clear ice' for simplicity. Yellow-coloured ice was distinctly yellow in colour and appeared as discrete layers within the naled cores. Five ice cores recorded these yellow-coloured ice layers, which ranged in thickness from 10-25 cm, at various depths (Fig. 7b, e; Fig. 8a, c, e). Yellow-coloured ice ~~did not appear~~was not found in any of the accreted ice cores. Sediment-rich ice had clear sediment inclusions that accounted for >50% of the core section. Sediment layers were present in nearly all core samples (except I2, I7 and I8), with more pronounced sediment-rich layers (between 10-40 cm thick) recorded in I1, I3, I5 and I10 (Fig. 7 and 8). These sediment-rich layers only appeared as discrete layers within the naled ~~cores~~cores, but they account for almost the full core length in the accreted ice cores (Fig. 3 and 4). Facies logs for each ice core and their resultant geochemical profiles are provided in Figures 7, 8 and 9.

Accreted ice cores were typically multi-metre in length and consisted of heavily sediment-laden ice (Fig. 4), which ~~). This ice~~ appeared~~s~~ to be a mix of frazil ice and silt to fine sand sediments. ~~and co~~Cores ranged in length from ~25 to 240 cm (Fig. 9). The longest core, A4, had no visible layers, but the full core was sediment-laden with clay to fine ~~sand sized~~sand-sized particles (~~see~~ Fig. 4d). Bands of opaque ice, less than 10 cm thick, were recorded at

various intervals throughout cores A1, A2 and A3~~. Aside from these intersections, all accreted ice cores exhibit similar sediment laden ice facies with tabular ice lenses (Fig. 4) and limited discernible differences between and within ice cores~~.

4.3. Geochemistry

Proportions of major ions and total dissolved solids (TDS) are shown for each core in Fig. 7, 8 and 9. The naled ice cores and their sub-naled waters display a range of ~~total dissolved solids (TDS)~~TDS concentrations, broadly spanning from very dilute (less than 1 mg L^{-1}) to highly concentrated (up to ~~1,300~~3,000 mg L^{-1}) depending on the core and depth. Across most cores, HCO_3^- is the dominant anion, while Ca^{2+} is consistently the most abundant cation. In general, we observe that ice layers with low TDS, such as ~~as those found throughout~~ naled I1 and ~~the lower portions of~~lower I7 (Fig. 7a~~.~~, Fig. 8b), are typically SO_4^{2-} poor (though sometimes NO_3^- enriched)~~. , and~~ Whereas very concentrated TDS ~~layers~~ such as the naled waters in I2 and I3 (Fig.7b and c) are more often SO_4^{2-} enriched~~. Naled waters from I2 and I3, exhibit~~ and have ~~substantially higher~~higher TDS concentrations than the overlying ice. ~~The geochemical composition of some of the naled waters are not represented in Fig.8, namely cores I8 and I10, as an unknown source of positive charge was detected causing a large change imbalance.~~

Naled cores I1, I7, I8, I11 and I12 were all located in the main proglacial river channel. ~~In terms of spatial differences, n~~Naled I1 was located closest to the glacier and ~~unique in that it was~~ extracted from beneath a layer of mud, whereas all other naled icings were collected from clean ice surfaces. ~~The upper layer of naled I1 with some sediment inclusions, had no detectable SO_4^{2-} and low TDS values of 2.5 mg L^{+} (Fig. 7a) Naled I1 was also the naled structure closest to the glacier margin and located in the main meltwater channel. Similarly, naled I7 and I8 (two samples taken from the same naled structure, Fig. 2a) and I11 were also located in the main channel. I12 was then sampled as a newly emerging naled with only a thin layer of domed ice extracted after it was observed to have begun forming in the main channel~~

~~overnight in March 2024. Here, the very surface of the naled ice was sampled and showed moderate TDS amounts of 16-18 mg L^{-1} with an almost even proportion of HCO_3^- and SO_4^{2-}, similar to the ion proportions seen in other naled ice cores (Fig. 9b).~~ All ~~of the~~ cores sampled from the main channel lack yellow ice layers ~~within the naled cores~~ apart from I8, ~~with~~ which had a distinct yellow layer at the very surface and yellow water at the base of the core (Fig. 8). These main channel cores generally exhibit moderate TDS concentrations, ~~with the exception of~~except I8, which reaches up to 1324~~0~~ mg L^{-1} at its base and 3,098 mg L^{-1} in the water. HCO_3^- dominance is consistent across all main channel cores, SO_4^{2-} contributions ~~remain~~ are relatively low compared to some side channel cores. NO_3^- is slightly more elevated in I8 than in the other main channel cores. I12 was sampled as a newly emerging naled with only a thin layer of domed ice extracted after it began forming in the main channel overnight in March 2024. Here, the very surface of the naled ice was sampled and showed moderate TDS concentrations of 24-40 mg L^{-1} with an almost even proportion of HCO_3^- and SO_4^{2-}.

Side channel cores, I2, I3, I4, I5, I6, I9 and I10 show greater variability in both TDS ~~amounts~~ concentrations (~~1~~2-500 mg L^{-1} in ice and ~~1,300~~2,100 mg L^{-1} in naled waters) and ion proportions. While HCO_3^- and Ca^{2+} ~~still~~ dominate ~~in many of these cores~~, SO_4^{2-} contributes more proportionally~~the proportion of ions~~ across several cores~~of them~~, most notably the naled water in I2, I6, and I10. Core I10 is particularly distinct, with SO_4^{2-} comprising over 40% of total ions throughout and TDS values reaching up to ~~500~~ 548 mg L^{-1} in the yellow ice layers. Naled waters sampled beneath I2 and I3 also show ~~substantially~~ higher TDS concentrations of ~~1,300~~2,030 mg L^{-1} and ~~890~~ 1,032 mg L^{-1}, respectively.

Accreted ice cores (A1-A4) are ~~much~~ more uniform ~~than naled ice cores~~ in their geochemical signature both within single cores and across cores (Fig. 9c-f). All cores have TDS concentrations between ~~7-30~~13 and 39 mg L^{-1} (Fig. 9c-f). HCO_3^- and Ca^{2+} consistently

Formatted: English (United Kingdom)

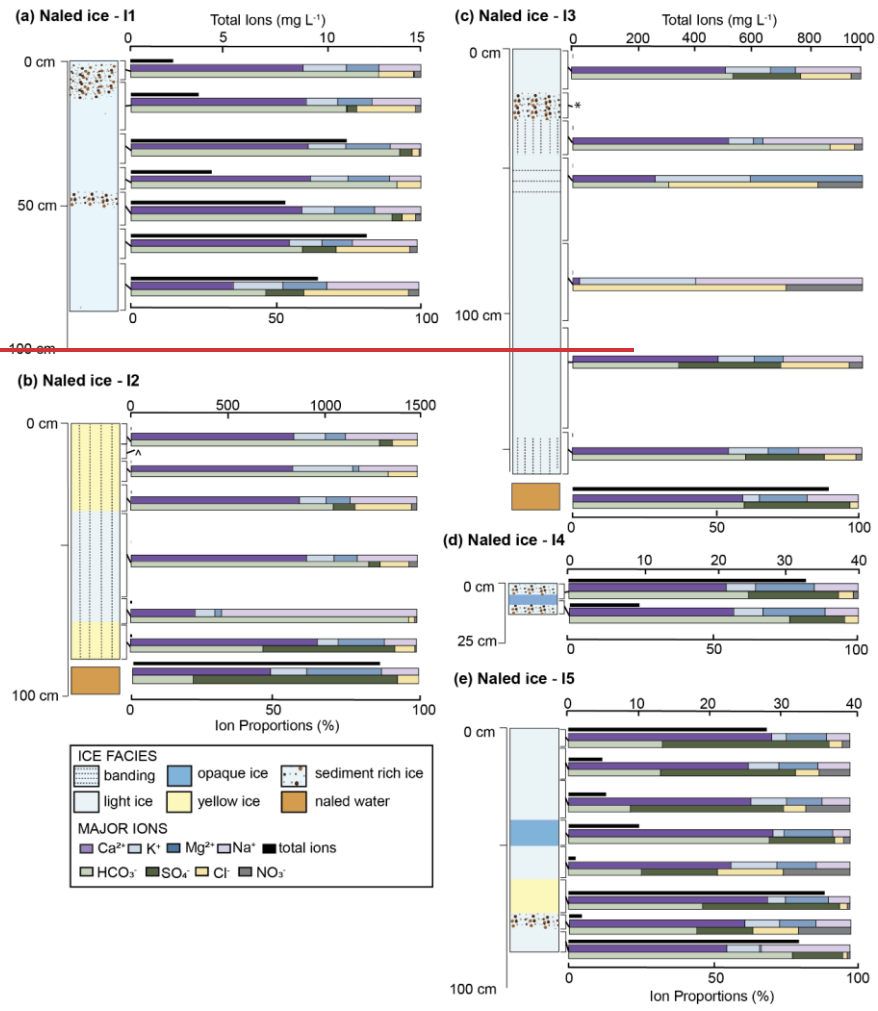
dominate, ~~throughout all of cores at~~comprising 50-80% of anion~~s~~ and cation proportion~~s~~, respectively. The most variability is seen in accreted core A4, where SO_4^- dominates the anions in some of the core sections. Accreted cores also have marginally higher proportions of K^+ compared to the naled ice cores.

Formatted: English (United Kingdom)

Formatted: English (United Kingdom)

Formatted: English (United Kingdom)

Formatted: English (United Kingdom)


(a) Naled ice - I1
Total Ions (mg L-1)
0 5 10 15
0 cm
50 cm
100 cm
0 50 100
(b) Naled ice - I2
0 500 1000 1500
0 cm
100 cm
0 50 100
Ion Proportions (%)
(c) Naled ice - I3
Total Ions (mg L-1)
0 200 400 600 800 1000
0 cm
100 cm
0 50 100
(d) Naled ice - I4
0 10 20 30 40
0 cm
25 cm
0 50 100
(e) Naled ice - I5
0 10 20 30 40
0 cm
100 cm
0 50 100
Ion Proportions (%)
ICE FACIES
banding
opaque ice
sediment rich ice
light ice
yellow ice
naled water
MAJOR IONS
Ca2+ K+ Mg2+ Na+ total ions
HCO3- SO4- Cl- NO3-

412

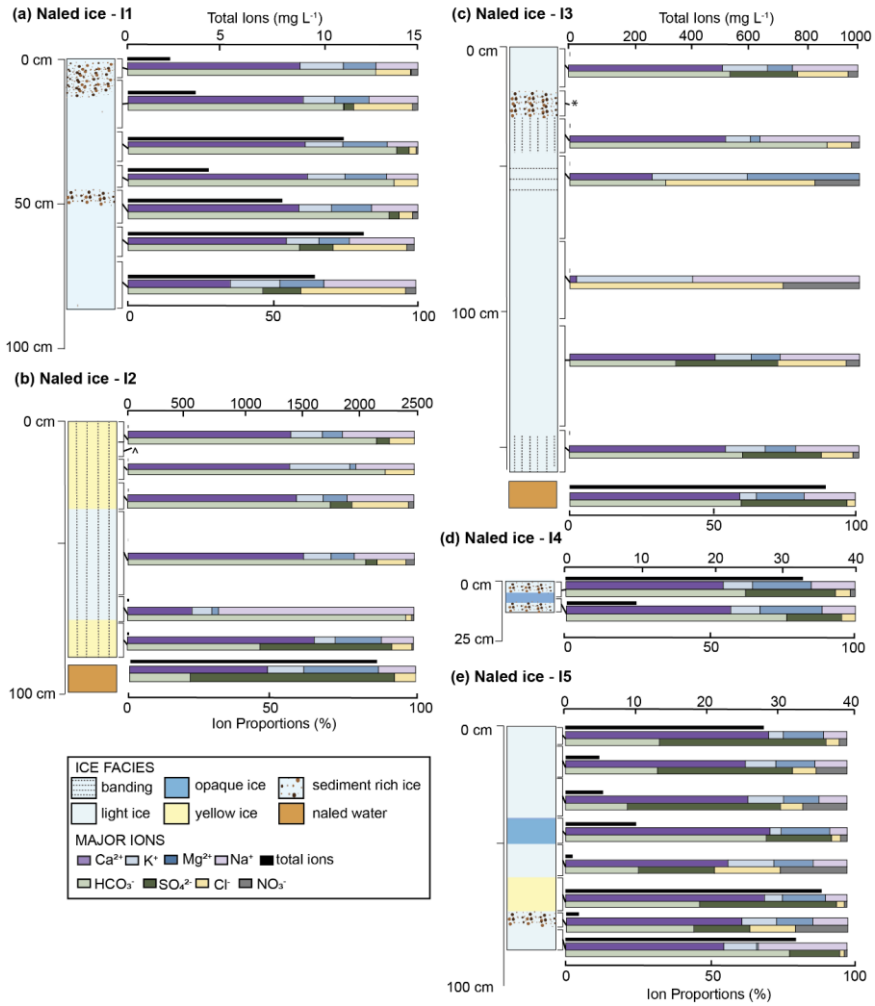
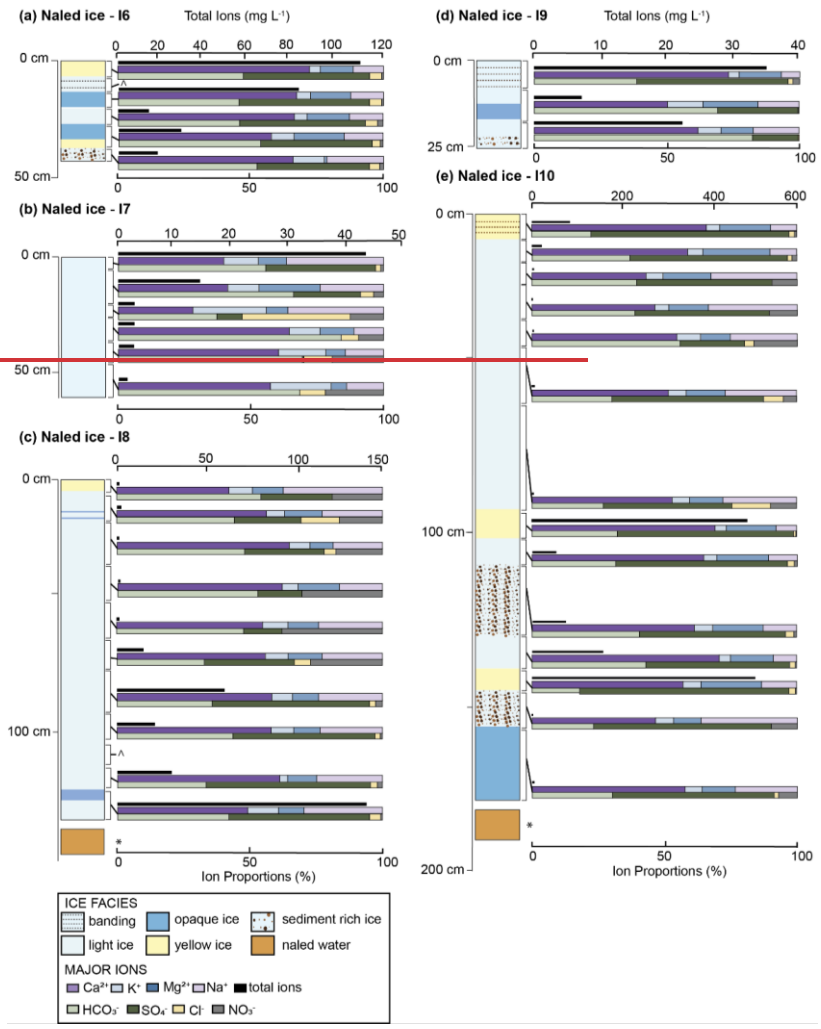
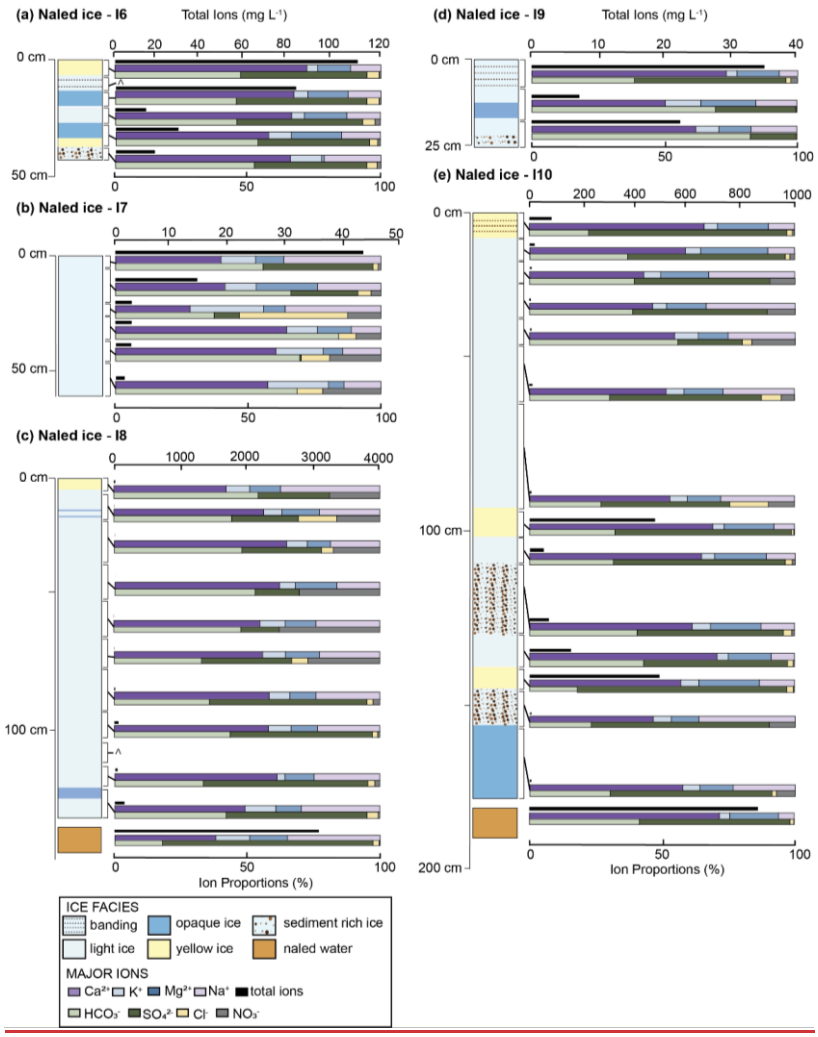


Figure 7 Ice facies and geochemical profiles of major ions for naled ice cores I1 through I5 collected April 2023 and March-April 2024. Vertical columns indicate ice facies types. Geochemical results are illustrated with cumulative horizontal bars adjacent to sampling depth (exact depth range indicated by black brackets). Total dissolved solids (TDS) are given in mg L^{-1} (upper, black bar); note unique axis values for each core. For some samples, values are so low, that they plot as a point. The proportions of cations (middle bar plot, Ca^{2+}, K^{+}, Mg^{2+}, and Na^{+}) and anions (lower bar plot, Cl^{-}, SO_4^{2-}, NO_3^{-}, and HCO_3^{-}) are given in percentages.

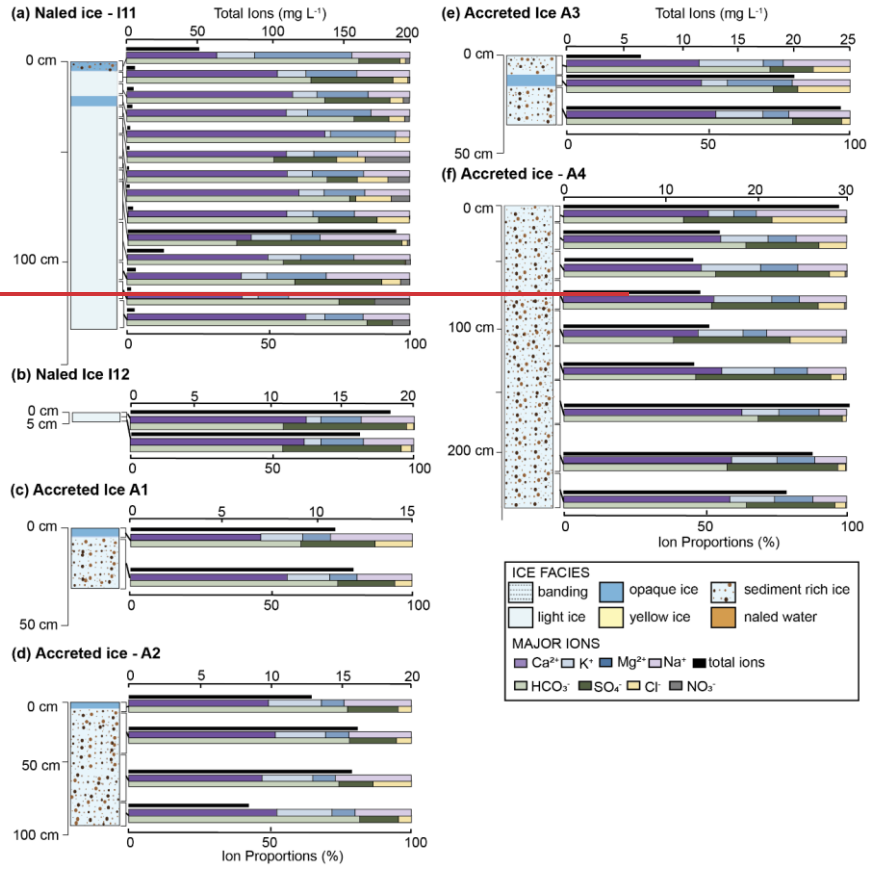

(a) Naled ice - I6
Total Ions (mg L⁻¹)
0 20 40 60 80 100 120
0 cm
50 cm
0 50 100
(b) Naled ice - I7
0 10 20 30 40 50
0 cm
50 cm
0 50 100
(c) Naled ice - I8
0 50 100 150
0 cm
100 cm
0 50 100
Ion Proportions (%)
(d) Naled ice - I9
Total Ions (mg L⁻¹)
0 10 20 30 40
0 cm
25 cm
0 50 100
(e) Naled ice - I10
0 200 400 600
0 cm
100 cm
200 cm
0 50 100
Ion Proportions (%)
ICE FACIES
banding
opaque ice
sediment rich ice
light ice
yellow ice
naled water
MAJOR IONS
Ca2+ K+ Mg2+ Na+ total ions
HCO3- SO4- Cl- NO3-

422



423

424 **Figure 8** Ice facies and geochemical profile of major ions for naled ice cores I6 through
425 I10 collected March-April 2024. Vertical columns indicate ice facies types and changes
426 with depth. Geochemical results are illustrated with cumulative horizontal bars adjacent
427 to sampling depth (exact depth range indicated by black brackets). TDS is given in mg L^{-1}
428 (upper bar; note unique charge range for each core) and the proportions of cations
429 (middle bar plot, Ca^{2+}, K^{+}, Mg^{2+}, and Na^{+}) and anions (lower bar plot, Cl^{-}, SO_4^{2-}, NO^{3-},
430 and HCO_3^{-}) are given in percentages. ~~*Naled water in core I8 and I10 has an unknown~~
431 ~~source of positive charge and is therefore not included in the graph.~~ ^Sample not analysed.


(a) Naled ice - I11
Total Ions (mg L-1)
0 50 100 150 200
0 cm
100 cm
0 50 100
(b) Naled Ice I12
0 5 10 15 20
0 cm
5 cm
0 50 100
(c) Accreted Ice A1
0 5 10 15
0 cm
50 cm
0 50 100
(d) Accreted ice - A2
0 5 10 15 20
0 cm
50 cm
100 cm
0 50 100
Ion Proportions (%)
(e) Accreted Ice A3
Total Ions (mg L-1)
0 5 10 15 20 25
0 cm
50 cm
0 50 100
(f) Accreted ice - A4
0 10 20 30
0 cm
100 cm
200 cm
0 50 100
Ion Proportions (%)
ICE FACIES
banding
opaque ice
sediment rich ice
light ice
yellow ice
naled water
MAJOR IONS
Ca2+ K+ Mg2+ Na+ total ions
HCO3- SO4- Cl- NO3-

432

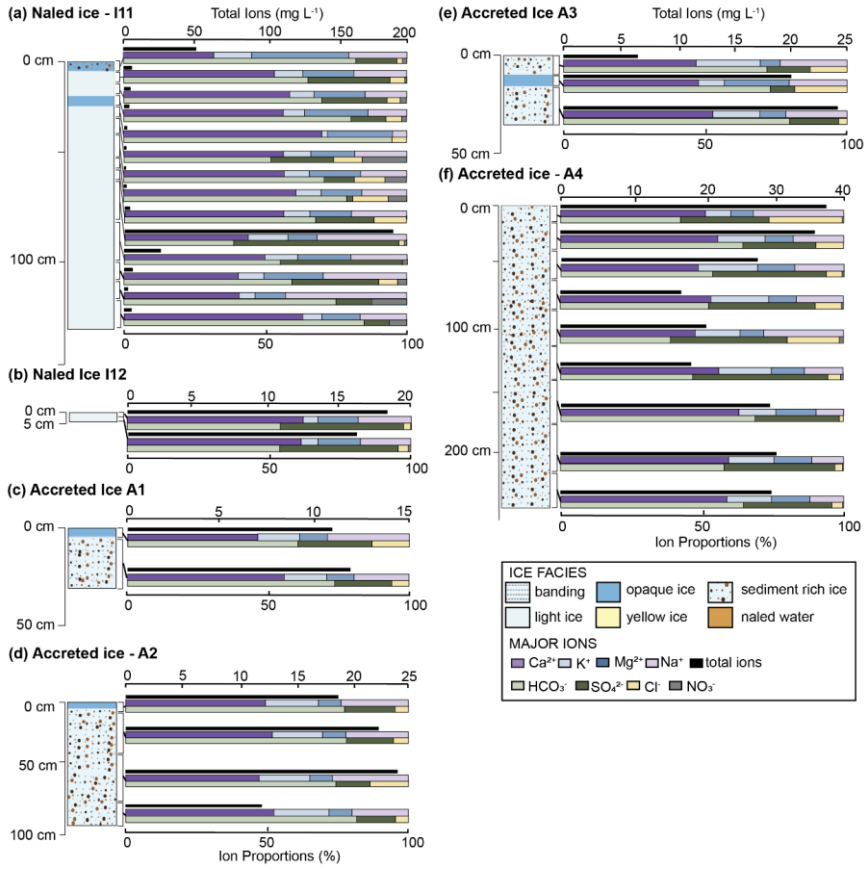


Figure 9 Ice facies and geochemical profile of major ions for naled ice cores I11 and I12 collected March-April ~~2024~~2024, and accreted ice cores collected October 2022 and April 2023. Vertical columns indicate ice facies types and changes with depth. Geochemical results are illustrated with cumulative horizontal bars adjacent to sampling depth (exact depth range indicated by black brackets). TDS ~~in~~ is given in mg L^{-1} (upper bar; note unique charge range for each core) and the proportions of cations (middle bar plot, Ca^{2+}, K^{+}, Mg^{2+}, and Na^{+}) and anions (lower bar plot, Cl^{-}, SO_4^{2-}, NO_3^{-}, and HCO_3^{-}) are given in percentages.

Formatted: Justified

4.4. Stable water isotopes

Isotopic compositions ($\delta^{18}O$ and δD) reveal ~~that~~ accreted ice samples ~~generally~~ have slightly higher $\delta^{18}O$ and δD values (Fig. 10a; -21±1.7 ‰) compared to naled ice (Fig. 10a; -24±2.3 ‰). Surface glacier ice plots separately from all naled samples with the lowest $\delta^{18}O$ value (-33.5 ‰), indicating the naled ice is distinctly different in water source and/or formation mechanism than surface glacier ice (Fig. 10a). Deuterium excess (*D-excess* = $\delta^2H - 8 \cdot \delta^{18}O$) values ~~were used to determine the role of evaporation or freezing processes on the water samples isotopic composition (Fig. 10b). Deuterium excess values~~ range from approximately 3 ‰ to 32 ‰ with a general trend of decreasing deuterium excess with increasing $\delta^{18}O$ values (Fig. 11).

~~Isotopic composition changes~~ Changed in isotopic composition were also observed down-cores, revealing potential freezing mechanisms. Within naled core I8 (Fig. 10b) $\delta^{18}O$ values generally decrease downcore (the lowest values detected at 132-146 cm of -29.5 ‰) ~~and~~ whereas deuterium excess ~~increasing~~ increases from 9.8 ‰ at the top of the core to 25 ‰ at the base~~, exhibiting~~ due to increasing fractionation processes downcore (Fig. 10b). However, a distinct but ~~small increase~~slight increase~~s~~ in $\delta^{18}O$ and decrease~~s~~ in deuterium excess ~~values are also seen~~was noted at 104-108 cm ~~mid core~~. When plotted on a freezing curve, naled ice samples I5, I8, I10 and I11 all display R^2 values of >0.9, suggesting sequential freezing downcore (Fig. 11). However, some core sections (in I2, I3, I4, I6, I7 and I9) do plot away from the freezing line with R^2 values of 0.07-0.93 (Fig. S4 in Supplementary Information). These sections ~~are representative of~~represent discrete intervals of an increase in $\delta^{18}O$ and decrease~~s~~ in deuterium excess (also seen in Fig.10b), suggesting the start of a new freezing package~~s~~.

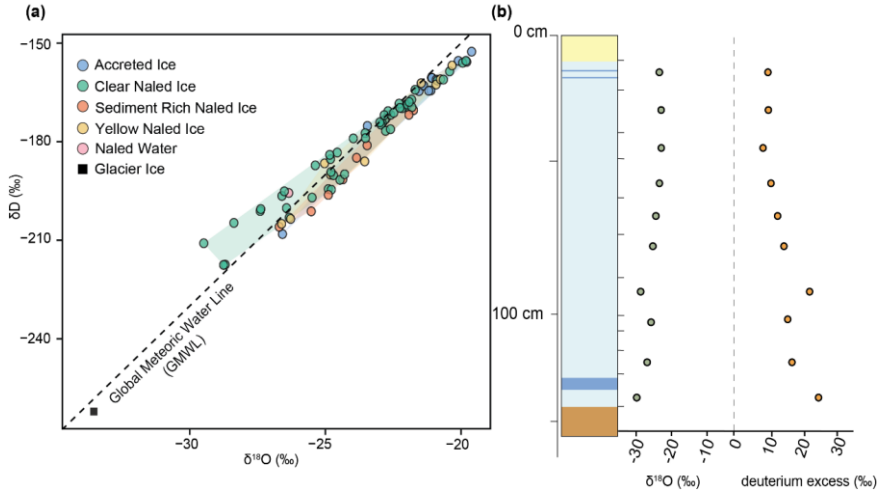


Figure 10 Summary of stable isotope ~~analysis~~ analyses of different ice types. (a) Cross-plot of δD vs $\delta^{18}O$ compared to the Global Meteoric Water Line (GMWL). (b) Down-core change in $\delta^{18}O$ (green points) and deuterium excess (orange points) in naled core I8. Shaded regions in a-c denote the range of isotope and chemical data for ice and water. Note, only a ~~select number~~subset of samples were analysed for stable water isotopes.

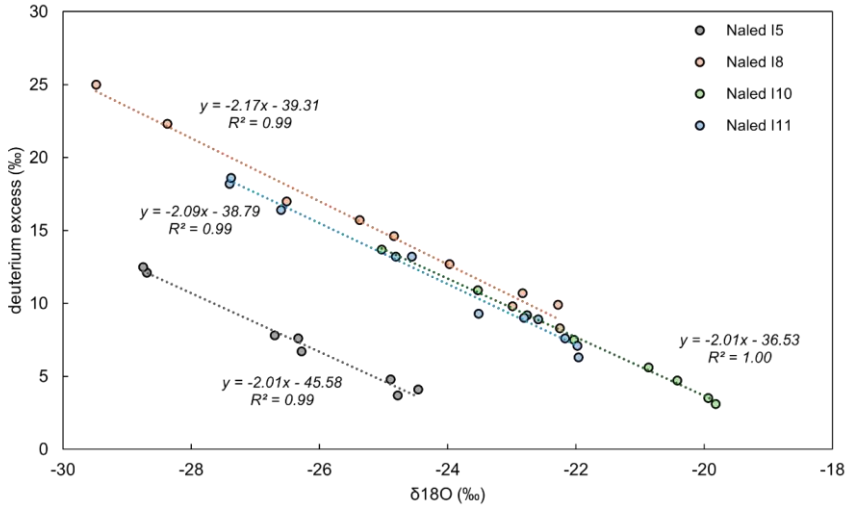


Figure 11 Cross-plot of deuterium excess vs $\delta^{18}O$ of naled ice samples I5, I8, I10 and I11 on hypothesised freezing curves. All samples plot along the freezing curve ~~in depth order~~ with increasing $\delta^{18}O$ and decreasing deuterium excess values with~~at~~ depth, indicative of sequential freezing downcore.

4.5. Electrical Resistivity Tomography

Electrical Resistivity Tomography (ERT) ~~experiments~~ surveys were conducted <400 m from the terminus of Isunnguata Sermia, in an area where gravel-rich sediments dominate (Fig. 2). ~~Our~~ The resulting ERT images (Fig. 12) reveal considerable spatial heterogeneity in subsurface resistivity, spanning from $\log_{10}\rho$ ~0.83 to >8.1. In both ERT profiles, the uppermost layer (~1 - 5 m below the surface) is dominated by high resistivity values ($\log_{10}\rho$ >10.5), ~~which are~~ often indicative of dry and (at least partially) frozen material (Kneisel et al., 2014). As the surface is dominated by unsaturated gravel-rich glacial outwash material and compacted till, we expect this uppermost subsurface layer is similar in character.

Beneath ~~this~~ the high resistivity layer, an intermediate zone (approximately 5–15 m below ground level) exhibits markedly lower resistivities ($\log_{10}\rho$ ~2 - 4), ~~with resistivity~~ varying across both profiles (yellow/white/blue colours in Fig. 12a). Bound by higher resistivity above and below, this zone likely represents a saturated sediment ~~zone~~ layer composed of sands/gravel and/or finer material or fractured bedrock (Palacky, 1987; Hauck & Kneisel, 2008; Reynolds 2011). Each of these materials can host groundwater, ice or subglacial meltwater. Localised zones of even lower resistivity ($\log_{10}\rho$ ~1- 2) are observed within this intermediate zone in both profiles (Fig. 12a, insets). Their geometry is suggestive of discrete pockets or conduits of moisture, potentially reflecting melting permafrost or glacial outflow pathways (e.g., Hauck & Kneisel, 2008). In both profiles, resistivity values abruptly return to $\log_{10}\rho$ ~10.5 and then $\log_{10}\rho$ ~10.6 Ωm beneath the intermediate zone. We interpret this to ~~represent~~ be drier sediments~~,~~ and/or frozen ground/ice (Kneisel et al., 2014), which ~~we deem~~would be likely in the forefield of Isunnguata Sermia in winter.

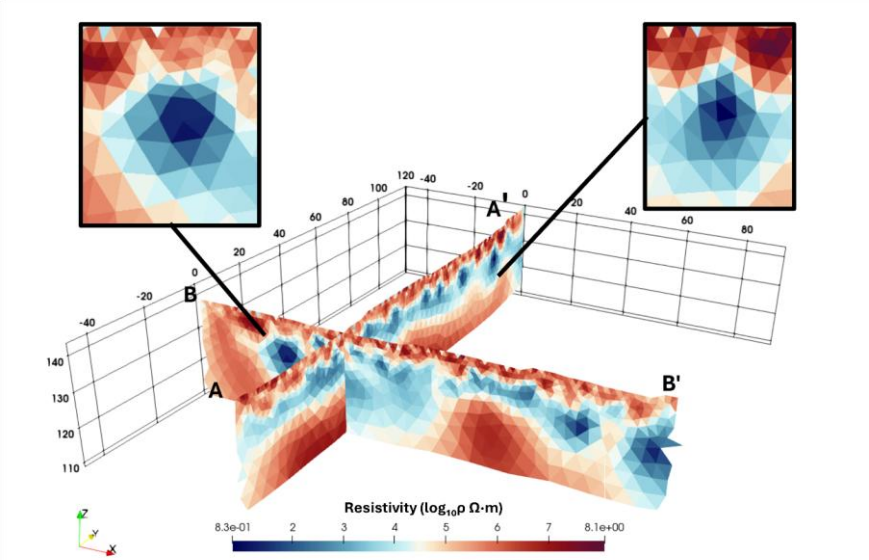


Figure 12 Two intersecting Electrical Resistivity Tomography (ERT) profiles surveyed in front of Isunnguata Sermia (location mapped on Figure 1). Depth and distance from starting location in metres. Resistivity values span a wide range (from $\log_{10}\rho$ ~1 to over 10.8), suggesting significant variations in moisture and/or porosity and/or liquid/frozen contrasts. Pockets of low resistivity, typical of high porosity or water-rich sediment zones, are shown in highlighted boxes.

5. Discussion

5.1. Naled ice formation mechanisms

~~Time-lapse~~Time-lapse camera footage, along with geochemical analyses of naledi and geophysical investigations of the glacial foreland at Isunnguata Sermia have allowed us to capture naledi ~~structures~~ formation mechanisms in unprecedented detail. Our data show icings forming under both confined and unconfined water input conditions.

In the confined condition, ice layers build up into dome-like structures, fed by the upwelling of waters from below (Fig. 5, 13). The waters likely originate from subglacial sources and are transported through subsurface conduits and/or saturated till (Fig. 12). In April 2024, naled ice domes were observed to have started forming overnight suggesting

that they may form ~~relatively~~ quickly (Fig. 5e). Following formation of an ice layer that restricts water flow, resultant build-up of water pressure beneath the naled can fracture the ice surface (e.g. Fig. 5c). The method of formation we describe here is akin to the formation mechanism described by Wadham et al.~~,~~ (2000) and Stachnik et al.~~,~~ (2016) (outlined in Fig. 1d-f).

Not all of the naledi studied were exclusively fed from waters below, and our results show that more than one formation mechanism exists with the incorporation of unconfined waters from, for example, englacial flow or precipitation. Automatic camera footage in Figure 5 ~~shows that~~demonstrates naledi ~~can also be~~being built from these unconfined waters, as ice layers accumulate from overland water flow ~~(beside upwellings)~~such as supra- and englacial melt and from local precipitation such as the snow ~~event~~event captured in the automatic cameras (Fig. 13). The cameras also captured the incorporation of yellow coloured waters originating off-camera. Due to the colour similarity with the waters collected below naled structures, we believe this overland flow originated from a large upwelling of overwinter waters at a nearby naled location. These camera-derived observations, combined with geochemical analysis, help to explain some of the unique ice facies we observed in the naled ice cores.

The waters with relatively high concentrations of TDS at the base of the naled cores are interpreted to reflect prolonged water storage in the subglacial system (at least over the winter months) - where chemical equilibration and mineral dissolution result in the highest TDS concentrations across our study site (e.g., Gokhman et al., 1987; Hodgkins et al., 2004; Stachnik et al., 2016; Yde et al., 2012). Layers of similar colours and geochemical signatures are also found within the naled cores such as I2, I8 and I10, suggestive of an eruptive process injecting these TDS-rich yellow coloured waters into the ice structure. Our geophysical analysis of the substrate supports ~~both of~~ these ideas,

as low resistivity TMS ~~returns are suggestive of~~suggests a saturated sediment layer ~~which~~ could be fed by subglacial meltwaters and/or groundwater. The geophysical survey ~~data interpretation~~ also identifies a potential conduit for water flow (~ 5 m in dia~~meter~~meter), which could efficiently transport subsurface waters over wintertime, contributing to naled ice structures when air temperatures limit overland flow.

The clear naled ice with low solute concentrations ~~suggest~~ suggests ~~water origins from~~ waters have had ~~with~~ limited mineral ~~surfaces~~surface contact for reactions to occur ~~on~~ (such as supra- or englacial melt/storage and/or overwinter precipitation). ~~These low solute waters form naled ice through relatively fast source to sink flow fed by proglacial meltwaters that haven't been transported through glacial till.~~ An alternative explanation is that these layers (most often found at the top of the naled cores) are partially frozen (or partially wasted) ice/slush, which just retains some of the solutes available - as the rest of the solutes have either run off completely (if unconfined), or moved downwards, where they have become concentrated in the bottom layer of the freezing package. For example, in I8 we see very low TDS values (0.8-1.2 mg L^{-1}) in the middle of the core, followed by giher concentrations of 15-141 mg L^{-1} further down the core, within the most isotopically enriched layers.~~An alternative explanation is that these layers, most often at the top of the naled cores are from only partially frozen (or partially wasted) ice/slush, with the ice retaining only some of the solutes and the rest of the solutes either running off (if unconfined) or being concentrated in the bottom layer of the freezing package. For example, in I8 we see very low TDS values (0.8-1.2 mg L^{-1}) in the middle of the core, followed by 15-141 mg L^{-1} further down the core and within the most isotopically enriched layers.~~

The downcore chemical and isotopic variation in naled ice can be explained, at least in part, by freezing processes. During freezing, ~~heavier isotopes freeze~~isotopically

572 enriched water freezes first, with a stronger effect on ^{2}H than ^{18}O. Remaining, freezing
573 water will fractionate on a freezing slope unlike that of meteoric water, controlled by the
574 initial composition of the water and the fractionation factors of freezing (Jouzel and
575 Souchez, 1982; Souchez and Jouzel, 1984). In a package of ice that froze in a single
576 outburst event, we expect the heaviest isotopes on the top and lighter isotopes downcore.
577 We also expect the concentration of dissolved solutes to significantly increase at the
578 bottom of a freezing package, from the effects of progressive freeze concentration of
579 dissolved solutes in the source water (Halde, 1980).
580

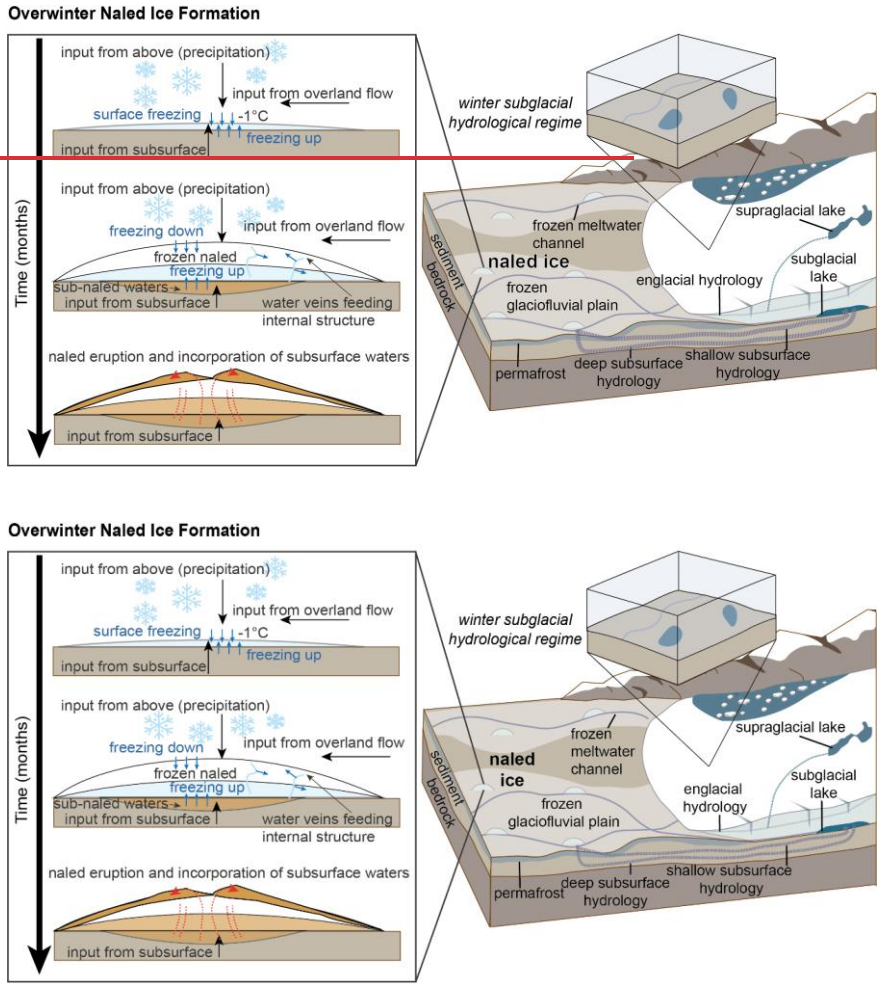


Figure 13. Conceptual diagram of naled ice formation mechanisms in western Greenland, based on ice facies, geochemical evidence and geophysical surveys of the proglacial area in front of Isunnguata Sermia. Inset box shows the evolution of naledi through winter, where water with long subsurface residence times ~~discharge~~ discharges into the proglacial forefield. Other water sources, such as supraglacial and englacial melt, also contribute to naled ice layers ~~freezing in sequences~~. Naledi in this area ~~incorporate~~ form from both bottom-up and top-down ~~formation~~ mechanisms – incorporating two existing theories of naled formation. Water upwellings ~~accrete~~ freeze onto the underside of the naled ice, and overland flow from supraglacial melt, englacial melt and precipitation ~~accrete~~ freeze on top of the ice~~, where layers of either water flow can build up over time (through the winter)~~.

The stable water isotopes ~~analysed here~~ reveal sequential freezing downcore with discrete freezing packages ~~likely~~ resulting from multiple upwelling events. These upwellings ~~freezing~~ freeze on at the base of existing ice, pushing up into ~~that existing~~the ice, and creating domed structures over wintertime. However, we also observe that in the top sections of some samples of ~~the~~ longer cores (I2 and I7) and the shorter cores below 50 cm (I3, I4, I6 and I9) ~~don't~~do not plot on this freezing curve ~~line~~. This ~~is suggestive of a~~indicates a different freezing sequence, potentially forming from a top-down process.

As water discharge is reduced over ~~these~~ the winter months, and less ~~capable of transporting~~ glacial sediment is transported~~s~~, the resulting naled ice is less sediment-laden than summer accreted ice, ~~formations~~ which ~~form~~ forms under faster water flow conditions (Fig. 13). We therefore conclude that the naledi on the forefield of Isunnguata Sermia form through a combination of unconfined and confined water sources~~.~~, where~~S~~ subsurface waters ~~which~~ emerge through the substrate overlain by ice ~~accumulate by freeze~~ freeze on below, whereas ~~water~~ overland flows and precipitation accumulate ~~progressively upward~~from above (Fig. 13).

5.2. Accreted ice formation mechanisms

The formation of accreted ice was captured on automatic cameras in the late melt season, September-October 2023, after a large upwelling event (Fig. 4; 6). Based on the speed of their formation ~~captured on cameras~~ and supported by our geochemical analyses, we propose that they form where supercooled meltwater is evacuated into the glacier forefield and quickly freezes ~~to form accreted ice during large eruption events during periods with cold surface temperatures~~ creating structures composed of a mix of frazil ice and silt to fine sand sediments (Fig. 14). ~~The ice accretions formed by the late melt season were observed to have persisted through the winter months preserved by cold temperatures, with gradual wastage evidenced by deflation and erosion of the ice surface~~

~~over the winter (likely due to discrete melt events), leaving behind large amounts of sediment accumulations. Due to our focus on overwinter ice accumulations, we were not present in the summer months to observe the complete wastage of accreted ice, however due to repeated field visits, accreted ice structures were observed to have formed in the same locations in subsequent years. This observation indicates that the subsurface plumbing system is stable on interannual timescales.~~

The accreted ice samples exhibit a moderately uniform geochemical signature throughout, where the cores are dominated by ~~sediment rich~~sediment-rich ice layers. This uniformity between sites~~,~~ and within each core suggests consistent water sources, potentially derived from single or time-constrained outflow events. These cores are also geochemically similar to previously characterised summer outflow waters in other studies (i.e., Graly et al., 2014; Graly et al., 2017a). Preserved by cold air temperatures, the ice accretions formed by the late melt season persist through the winter months, although gradual wastage is evidenced by deflation and erosion of the ice surface towards the end of the winter (due to discrete melt events), where melting leaves behind large sediment accumulations. Due to our focus on overwinter ice accumulations, we were not present in the summer months to observe the complete wastage of accreted ice; however, our repeat field campaigns allow us to note that accreted ice structures form in almost the exact same location each year. This observation indicates that the subsurface hydrological system must be stable over interannual timescales.

The subglacial hydrological system in this region ~~is thought to provide~~drives fast-moving, highly pressurised subglacial waters into the proglacial field~~—~~, generating large upwellings ~~which gush up to~~ several metres in ~~heigh~~ height during summer months (Graly et al., 2017a). This water is presumably routed through the deep subglacial trough beneath

Formatted: Indent: First line: 1.27 cm

Isunnguata Sermia (Lindbäck et al., 2015), where water will accumulate and interact with sediments and bedrock, before being driven up the reverse bed slope by high water pressure (when the subglacial hydrological system reaches capacity) (Cook et al., 2006; Lindbäck et al., 2014). The subsurface here is likely to be very ~~high porosity~~high-porosity sand/gravel deposited during the Holocene ice margin retreat ~~and,~~ which ~~favors~~ favours 'groundwater' flow and not ~~channelized~~ channelised flow. These highly pressurised supercooled waters then freeze into large icing structures close to minimal meltwater output zones at the glacier terminus (Fig. 6, 14). Currently, the growth and wastage rates of this accreted ice formation ~~is~~ are unknown, ~~however~~ though we observed that sporadic ~~hours~~ hours- to days-long upwelling events contribute to the majority of the ice formation (Fig. 6a-c). We hypothesise, based on the results presented here that the formation timescale is likely fast with sudden upwellings of high velocity, highly pressurised waters erupt into the glacial forefield (Fig. 14). Where these structures are formed from single outburst events in the late summer season, they may also incorporate waters from sub-, supra- and ice-marginal lakes where their outbursts are the primary source of the upwelling (e.g., Livingstone et al., 2026).

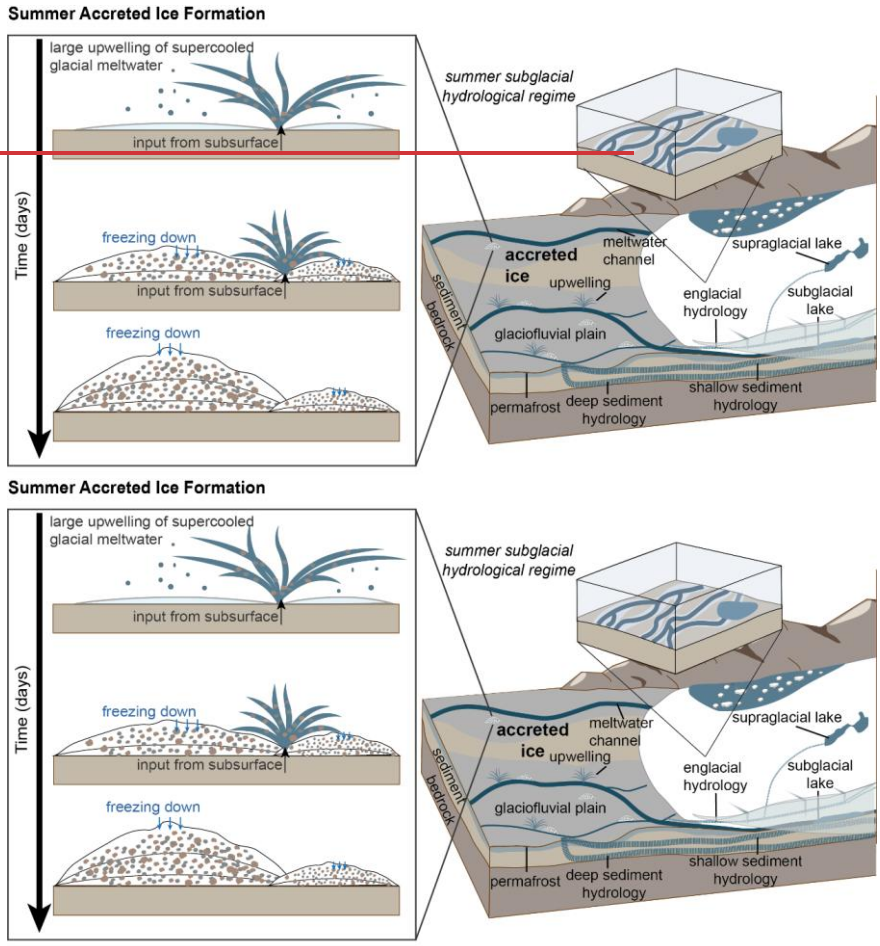


Figure 14 Conceptual diagram of accreted ice formation mechanisms in front of Isunnguata Sermia, Greenland, based on ice facies, geochemical evidence and geophysical surveys of the glacier foreland. Over summer, an efficient subglacial hydrological system moves sediment-loaded waters with low ion concentrations through subsurface ~~water flow~~hydrological pathways. This allows accreted ice to form where upwellings of highly pressurised supercooled waters erupt into the forefield and freeze adjacent to the upwelling in an isolated event ~~(see development of accreted ice structures in the inset panel)~~.

5.3. Implications and comparisons with existing formation theories

Previous theories of naled formation have adapted either a top-down or bottom-up approach (Fig. 1). One approach details growth from waters below icing structures, with

liquid water conduits within naled ice providing transport pathways insulated from the cold surface (Fig. 1f) (Stachnik et al., 2016; Wadham et al., 2000). The other approach ~~focusses~~ describes ~~on~~ accumulations from above where the cold, winter ~~atmosphere~~ air temperature acts as a heat sink, freezing any waters or precipitation that accumulate from above (Fig. 1a-c) (Schohl and Ettema, 1986; Yde et al., 2012). Our observations and results ~~supports~~support both of these existing theories. Winter-forming naledi at ~~our study site in Greenland~~Isunnguata Sermia form through a combination of top-down and bottom-up freezing processes, whilst summer accreted ice structures form by freeze-on of higher velocity, supercooled waters erupting onto the glacier foreland ~~when surface temperatures are cold~~.

These systems offer insights into hydrological systems in Greenland that are difficult to ~~ascertain~~ observe ~~from~~ by other means. They also show how water routing can vary spatially and temporally through the melt season. Geochemical differences in ice samples also raise important questions ~~related to~~for ~~nutrient supply and TDS~~solute and nutrient release from the Greenland Ice Sheet. With pronounced peaks in TDS detected in the overwinter naled waters, ~~year round~~year-round analyses of glacial waters ~~is~~ are critical for capturing the full extent of foreland water flow and the impact of these waters on downstream ecosystems, particularly at the release of these solute-rich waters during the initial onset of the melt season. ~~Indeed, t~~The seasonal changes in geochemistry we observe suggest that ~~nutrient export~~ solute export in winter may be under-represented in existing literature, ~~with important implications for our understanding~~which should be considered for a thorough understanding of biogeochemical processes and ~~their~~ wider ecosystem effects downstream (Hawkings et al., ~~2025~~2026).

6. Conclusions

~~Previous research on proglacial icings, primarily on Svalbard, have proposed distinct formation mechanisms for the generation of winter naled ice structures.~~ Over the course of four field seasons, we have investigated the formation and build-up of winter-forming naledi and ~~summer forming~~summer-forming accreted ice together for the first time, at ~~the proglacial forefield of~~ Isunnguata Sermia, ~~in~~ western Greenland. Using 15 ice cores, we geochemically characterised these ice structures for major ion and trace element concentrations, as well as δ^2H and $\delta^{18}O$ isotopic composition. By combining geochemistry with geophysical surveys and automatic camera footage, we can fully characterise and interpret icings~~,~~ and the hydrological pathways that drive their formation at Isunnguata Sermia for the first time. The different geochemical signatures and the stratification of ice layers in the naled cores we extracted and analysed suggest that there are multiple water sources and pathways which contribute to naled formation at Isunnguata Sermia. We detected several distinct water types within the naledi, from highly concentrated naled bottom waters ~~–~~enriched in dissolved ions (originating from deep hydrological sources and/or groundwater), through to extremely dilute naled ice layers that most likely originate from supraglacial or englacial waters (which have had limited time and/or opportunity for sediment-water interaction). Our findings demonstrate how naledi can form through a combination of top-down and bottom-up freeze-on processes, where water is supplied from a variety of water sources. We suspect that similar mechanisms will create naledi elsewhere, though one process may dominate over another depending on local conditions (e.g. ice/bed topography, meltwater availability, ground conditions). In contrast, the summer accreted ice ~~we observe at Isunnguata Sermia~~ is much less geographically diverse, implying supercooled waters from the same (or similar) sources freeze-on quickly, presumably during more discrete, ~~high output~~high-output events. By analysing icings ~~year round~~year-round, we record a

clear hydrological transition at Isunnguata Sermia, between summer (where supercooled waters emerge from efficient channelised drainage systems at pressure)~~,~~ and winter (where more inefficient distributed drainage networks dominate). ~~.—~~These seasonal changes drive different geochemical ~~and nutrient~~ outputs from ~~water flows of~~ the Greenland Ice Sheet~~, which can inform us about inland conditions which are hard to obtain through other means~~. Our observations demonstrate the importance of seasonality in solute availability and show the importance of measuring glacier meltwater contributions to proglacial groundwater systems and downstream ecosystems over longer study intervals.~~Our observations are critical for evaluating glacier meltwater contributions to proglacial groundwater systems and downstream ecosystems, quantifying the seasonality associated with changes in solute availability and flux.~~

Data Availability

Supplementary information including all geochemical and isotope data and automatic camera GIFs are available at Zenodo doi: 10.5281/zenodo.23159526 ~~at OSF doi:~~as supplementary material. Photographs of individual ice cores and detailed methodologies are provided alongside this manuscript.~~ https://doi.org/10.17605/OSF.IO/A4QZK. Photographs of individual ice cores and detailed methodologies are provided alongside this manuscript.~~

Author Contributions

Conceptualisation – JG, KW, WPG, TLH, KL

Data Curation – RM, JG, CLH, KW, WPG, TLH, MJ, JRH, FN, AMR, MT, TMT, KWo, BK, SM, HB, TK, AM, KL

Formal Analysis – RM, JG, KW, FN, MT, TMT, BK, SM, HB

Funding Acquisition – JG, KW, WPG, TLH, KL

Formatted: Body, Justified

Investigation – RM, JG, CLH, KW, WPG, TLH, MJ, JRH, FN, AMR, MT, TMT, KW, BK, SM, HB, TK, AM, KL

Methodology – RM, JG, KW, FN, MT, TMT, BK, SM, HB

Visualisation – RM, JG, KW, FN, MT, BK

Writing Original Draft – RM, JG, KW, FN

Writing Review and Editing – RM, JG, CLH, KW, WPG, TLH, MJ, JRH, FN, AMR, MT, TMT, KW, BK, SM, HB, TK, AM, KL

Competing Interests

The authors declare that they have no conflict of interest.

Acknowledgements

This work was funded by NSF-NERC grant OPP-2039854 and NE/W004860/1. The authors would like to acknowledge the support of Kangerlussuaq International Science Support (KISS) ~~, the Polar Geospatial Center for satellite imagery,~~ and Peter Braddock for field safety support. Geospatial support for this work provided by the Polar Geospatial Center under NSF-OPP grant OPP-2039854. The authors would also like to acknowledge Northumbria University's parental leave scheme, which provided research funding cover for KW.

Formatted: Font: Not Italic

Formatted: Font: Not Italic

References

Alley, R. B., Lawson, D. E., Evenson, E. B., Strasser, J. C., and Larson, G. J.: Glaciohydraulic supercooling: a freeze-on mechanism to create stratified, debris-rich basal ice: II. Theory, Journal of Glaciology, 44, 563-569, 10.3189/S0022143000002070, 1998.

770 Bartholomew, I., Nienow, P., Sole, A., Mair, D., Cowton, T., Palmer, S., and Wadham,
771 J.: Supraglacial forcing of subglacial drainage in the ablation zone of the Greenland ice
772 sheet, Geophysical Research Letters, 38, 8, 10.1029/2011GL047063, 2011a.
773 Bhatia, M. P., Das, S. B., Xu, L., Charette, M. A., Wadham, J. L., and Kujawinski, E. B.:
774 Organic carbon export from the Greenland ice sheet, Geochimica et Cosmochimica Acta,
775 109, 329-344, 10.1016/j.gca.2013.02.006, 2013.
776 Blanchy, G., Saneiyan, S., Boyd, J., McLachlan, P., and Binley, A.: ResIPy, an intuitive
777 open source software for complex geoelectrical inversion/modeling, Computers &
778 Geosciences, 137, 104423, 10.1016/j.cageo.2020.104423, 2020.
779 Carey, K. L.: Icings developed from surface water and ground water, 1973.
780 Chandler, D. M., Wadham, J. L., Lis, G. P., Cowton, T., Sole, A., Bartholomew, I.,
781 Telling, J., Nienow, P., Bagshaw, E. B., Mair, D., Vinen, S., and Hubbard, A.: Evolution
782 of the subglacial drainage system beneath the Greenland Ice Sheet revealed by tracers,
783 Nature Geoscience, 6, 195-198, 10.1038/NGEO1737, 2013.
784 Chu, W., Schroeder, D. M., Seroussi, H., Creyts, T. T., Palmer, S. J., and Bell, R. E.:
785 Extensive winter subglacial water storage beneath the Greenland Ice Sheet, Geophysical
786 Research Letters, 43, 12-484, 10.1002/2016GL071538, 2016.
787 Cook, S. J., Waller, R. I., Knight, P. G., and Simon J. Cook, R. I. W., Peter G. Knight:
788 Glaciohydraulic supercooling: the process and its significance, Progress in Physical
789 Geography, 30, 577-588, 10.1177/0309133306071141, 2006.
790 Evenson, E. B., Lawson, D. E., Strasser, J. C., Larson, G. J., Alley, R. B., Ensminger, S.
791 L., and Stevenson, W. E.: Field evidence for the recognition of glaciohydrologic
792 supercooling, Glacial Processes Past and Present, 10.1130/0-8137-2337-X.23, 1999.

793 Gokhman, V. V., Gokhman, V. V., and Gokhman, V. V.: Distribution and conditions of
794 formation of glacial icings on Spitsbergen, Polar Geography, 249-260,
795 10.1080/10889378709377334, 1987.
796 Graly, J., Harrington, J., and Humphrey, N.: Combined diurnal variations of discharge
797 and hydrochemistry of the Isunnguata Sermia outlet, Greenland Ice Sheet, The
798 Cryosphere, 11, 1131-1140, 10.5194/tc-11-1131-2017, 2017a.
799 Graly, J. A., Drever, J. I., and Humphrey, N. F.: Calculating the balance between
800 atmospheric CO2 drawdown and organic carbon oxidation in subglacial hydrochemical
801 systems, Global Biogeochemical Cycles, 31, 709-727, 10.1002/2016GB005425, 2017b.
802 Graly, J. A., Humphrey, N. F., and Harper, J. T.: Chemical depletion of sediment under
803 the Greenland Ice Sheet, Earth Surface Processes and Landforms, 41, 1922-1936,
804 10.1002/esp.3960, 2016.
805 Graly, J. A., Humphrey, N. F., and Licht, K. J.: Two Metrics Describing the Causes of
806 Seasonal and Spatial Changes in Subglacial Aqueous Chemistry, Frontiers in Earth
807 Science, 6, 195, 10.3389/feart.2018.00195, 2018.
808 Halde, R.: Concentration of impurities by progressive freezing, Water Research 14, 575-
809 580, 10.1016/0043-1354(80)90115-3, 1980
810 Harden, D., Barnes, P., and Reimnitz, E.: Distribution and Character of Naleds in
811 Northeastern Alaska, Arctic, 30, 28-40, 1977.
812 Hauck, C. and Kneisel, C.: *Applied geophysics in periglacial environments* (Vol. 10).
813 Cambridge University Press, 2008.
814 Hawkings, J.R., Bradley, J.A., Doting, E.L., Hassan, N., Hendry, K.R., Holt, A.D., Hood,
815 E., Spencer, R.G., Stibal, M., Tranter, M. and Venturelli, R.A.: Glacier biogeochemical
816 cycling and downstream impacts. *Nature Reviews Earth & Environment*, 1-20,
817 10.1038/s43017-025-00751-1, ~~2025~~2026.

Hawkings, J., Wadham, J., Tranter, M., Telling, J., Bagshaw, E., Beaton, A., Simmons, S.-L., Chandler, D., Tedstone, A., and Nienow, P.: The Greenland Ice Sheet as a hot spot of phosphorus weathering and export in the Arctic, Global Biogeochemical Cycles, 30, 191-210, 191-210, 10.1002/2015GB005237, 2016.

Hodgkins, R., Tranter, M., and Dowdeswell, J. A.: The Characteristics and Formation of ~~A~~a High-Arctic Proglacial Icing, Geografiska Annaler Series A-physical Geography, 86(3), 265-275, 10.1111/j.0435-3676.2004.00230.x, 2004.

Jouzel, J. and Souchez, R. A.: Melting–Refreezing at the Glacier Sole and the Isotopic Composition of the Ice, Journal of Glaciology, 28, 35-42, 10.3189/S0022143000011771, 1982.

Kane, D. L.: Physical mechanics of aufeis growth, Canadian Journal of Civil Engineering, 8, 186-195, 1981.

Kneisel, C., Emmert, A. and Kästl, J.: Application of 3D electrical resistivity imaging for mapping frozen ground conditions exemplified by three case studies. *Geomorphology*, *210*, 71-82, 10.1016/j.geomorph.2013.12.022, 2014

Krawczyk, W.E., Lefauconnier, B. and Pettersson, L.E.: Chemical denudation rates in the Bayelva catchment, Svalbard, in the fall of 2000. *Physics and Chemistry of the Earth, Parts A/B/C*, *28*(28-32), 1257-1271, 10.1016/j.pce.2003.08.054, 2003.

Lawson, D. E., Strasser, J. C., Evenson, E. B., Alley, R. B., Larson, G. J., and Arcone, S. A.: Glaciohydraulic supercooling: a freeze-on mechanism to create stratified, debris-rich basal ice: I. Field evidence, Journal of Glaciology, 44, 547-562, 10.3189/S0022143000002069, 1998.

Lawson, E. C., Wadham, J. L., Tranter, M., Stibal, M., Lis, G. P., Butler, C. E. H., Laybourn-Parry, J., Nienow, P., Chandler, D., and Dewsbury, P.: Greenland Ice Sheet

842 exports labile organic carbon to the Arctic oceans, Biogeosciences, 11, 4015-4028,
843 10.5194/bg-11-4015-2014, 2014.
844 Lindbäck, K., Pettersson, R., Hubbard, A. L., Doyle, S. H., As, D., Mikkelsen, A. B., and
845 Fitzpatrick, A. A.: Subglacial water drainage, storage, and piracy beneath the Greenland
846 ice sheet, Geophysical Research Letters, 42, 7606-7614, 10.1002/2015GL065393, 2015.
847 Lindbäck, K., Pettersson, R., Doyle, S. H., Helanow, C., Jansson, P., Kristensen, S. S.,
848 Stenseng, L., Forsberg, R., and Hubbard, A. L.: High-resolution ice thickness and bed
849 topography of a land-terminating section of the Greenland Ice Sheet, Earth System
850 Science Data, 6, 331-338, 10.5194/essd-6-331-2014, 2014.
851 Livingstone S., Storrar R., Doyle S., Thorpe S., Moffatt A., Sole A., Chudley T. R.,
852 Gimbert F., Graly J., Licht K., Winter K., Jayarapu, A., Bagshaw, E., Barruol, G., Bauer,
853 K., Bianchi, G., Buzzard, S., Clason, C., Craw, L., Davison, B., Edwards, L., Gilhooly,
854 W., Hamilton, T. L., Hansen, C., Hawkins, J., Ing, R., Jatta, M., Jones, A., Kennedy, T.,
855 Killingbeck, S., Le Bris, T., McCerery, R., Messerli, A., Michel, A., Napoleoni, F.,
856 Peacey, M., Prior-Jones, M. R., Ross, N., Veness, R., Hepburn, A., Booth, A. Ice
857 dynamic and hydrological response to ice-dammed lake drainages at Isunnguata Sermia,
858 West Greenland, Journal of Glaciology, 2026.
859 Livingstone, S. J., Sole, A. J., Storrar, R. D., Harrison, D., Ross, N., and Bowling, J.:
860 Brief communication: Subglacial Lake drainage beneath Isunguata Sermia, West
861 Greenland: geomorphic and ice dynamic effects, The Cryosphere, 13, 2789-2796,
862 10.5194/tc-13-2789-2019, 2019.
863 Mallinson, L., Swift, D. A., and Sole, A. J.: Proglacial icings as indicators of glacier
864 thermal regime: ice thickness changes and icing occurrence in Svalbard, Geografiska
865 Annaler Series A-physical Geography, 101(4), 334-349,
866 10.1080/04353676.2019.1670952, 2019.

867 Meierbachtol, T., Harper, J., and Humphrey, N.: Basal drainage system response to
868 increasing surface melt on the Greenland Ice Sheet, Science, 341, 777-779,
869 10.1126/science.1235905, 2013.
870 Meire, L., Meire, P., Struyf, E., Krawczyk, D. W., Arendt, K. E., Yde, J. C., Pedersen, T.
871 J., Hopwood, M. J., Rysgaard, S., and Meysman, F. J. R.: High export of dissolved silica
872 from the Greenland Ice Sheet, Geophysical Research Letters, 43, 9173-9182,
873 10.1002/2016GL070191, 2016.
874 Morse, P. D. and Wolfe, S. A.: Geological and meteorological controls on icing (aufeis)
875 dynamics (1985 to 2014) in subarctic Canada, Journal of Geophysical Research: Earth
876 Surface, 120, 1670-1686, 10.1002/2015JF003534, 2015.
877 Pain, A. J., Martin, J. B., Martin, E. E., Rennermalm, Å. K., and Rahman, S.:
878 Heterogeneous CO2 and CH4 content of glacial meltwater from the Greenland Ice Sheet
879 and implications for subglacial carbon processes, The Cryosphere, 15, 1-33, 10.5194/tc-
880 15-1627-2021, 2021.
881 Palacky, G.J.: Resistivity characteristics of geologic targets, In: Electromagnetic methods
882 in applied geophysics, 10.1190/1.9781560802631.ch3, 1987
883 Pitcher, L. H., Smith, L. C., Gleason, C. J., Miège, C., Ryan, J. C., Hagedorn, B., van As,
884 D., Chu, W., and Forster, R. R.: Direct observation of winter meltwater drainage from the
885 Greenland Ice Sheet, Geophysical Research Letters, 47, e2019GL086521,
886 10.1029/2019GL086521, 2020.
887 Porter, C., Howat, I., Noh, M.J., Husby, E., Khuvis, S., Danish, E., Tomko, K., Gardiner,
888 J., Negrete, A., Yadav, B., Klassen, J., Kelleher, C., Cloutier, M., Bakker, J., Enos, J.,
889 Arnold, G., Bauer, G., and Morin, P., 2023, "ArcticDEM – Mosaics, Version 4.1",
890 https://doi.org/10.7910/DVN/3VDC4W, Harvard Dataverse, V1, [01/09/2024].

Reynolds, J.M.: An introduction to applied and environmental geophysics. John Wiley & Sons., 2011

Roberts, M. J., Russell, A. J., Tweed, F. S., and Knudsen, Ó.: Controls on englacial sediment deposition during the November 1996 jökulhlaup, Skeiðarárjökull, Iceland, Earth Surface Processes and Landforms, 26, 935-952, 10.1002/esp.236, 2001.

Roberts, M. J., Tweed, F. S., Russell, A. J., Knudsen, O. ~~.~~S., Lawson, D. E., Larson, G. J., Evenson, E. B., and Björnsson, H.: Glaciohydraulic supercooling in Iceland, Geology, 30, 871-874, 10.1130/0091-7613(2002)030, 2002.

Schohl, G. A. and Ettema, R.: Theory and Laboratory Observations of Naled Ice Growth, Journal of Glaciology, 32, 168-177, 10.3189/S0022143000015483, 1986.

Sobota, I.: Icings and their role as an important element of the cryosphere in High Arctic glacier forefields, Bulletin of Geography: Physical Geography Series, 81-93, 10.1515/bgeo-2016-0006, 2016.

Sodemann, H., Mørkved, P. T., and Wahl, S.: FLIIMP - a community software for the processing, calibration, and reporting of liquid water isotope measurements on cavity-ring down ~~spectrometers~~spectrometers, MethodsX, 11, 102297, 10.1016/j.mex.2023.102297, 2023.

Souchez, R. A. and Jouzel, J.: On the Isotopic Composition in δD and δ18O of Water and Ice During Freezing, Journal of Glaciology, 30, 369-372, 10.3189/S0022143000006249, 1984.

Stachnik, L., Yde, J. C., Kondracka, M., D., I., and Grzesik, M.: Glacier naled evolution and relation to the subglacial drainage system based on water chemistry and GPR surveys (Werenskioldbreen, SW Svalbard), Annals of Glaciology, 57, 19-30, 10.1017/aog.2016.9, 2016.

van Gool, J. A. M., Connelly, J. N., Marker, M., and Mengel, F. C.: The Nagssugtoqidian Orogen of West Greenland: Tectonic evolution and regional correlations from a West Greenland perspective, Canadian Journal of Earth Science, 39, 665-686, 10.1139/E02-027, 2002.

Wadham, J. L., Tranter, M., and Dowdeswell, J. A.: Hydrochemistry of meltwaters draining a polythermal-based, high-Arctic glacier, south Svalbard: II. Winter and early Spring, Hydrological Processes, 14, 1767-1786, 10.1002/1099-1085(200007)14:10<~~1767::~~1767:aid-hyp103>3.0.co;2-q, 2000.

Wadham, J. L., Hawkings, J., Telling, J., Chandler, D., Alcock, J., O'Donnell, E., Kaur, P., Bagshaw, E., Tranter, M., Tedstone, A., and Nienow, P.: Sources, cycling and export of nitrogen on the Greenland Ice Sheet, Biogeosciences, 13, 6339-6352, 10.5194/bg-13-6339-2016, 2016.

Weng, Y., Touzeau, A. and Sodemann, H.: Correcting the impact of the isotope composition on the mixing ratio dependency of water vapour isotope measurements with cavity ring-down ~~spectrometers~~spectrometers, Atmospheric Measurement Techniques, 13(6), 3167-3190, 2020.

Yde, J. C., Knudsen, N. T., Hasholt, B., and Mikkelsen, A. B.: Meltwater chemistry and solute export from a Greenland Ice Sheet catchment, Watson River, West Greenland, Journal of Hydrology, 519, 2165-2179, 10.1016/j.jhydrol.2014.10.018, 2014.

Yde, J. C., Hodson, A. J., Solovjanova, I., Steffensen, J. P., Nørnberg, P., Heinemeier, J., and Olsen, J.: Chemical and isotopic characteristics of a glacier-derived naled in front of Austre Grønfjordbreen, Svalbard, Polar Research, 31, 17628, 10.3402/polar.v31i0.17628, 2012.

938 Yoshikawa, K., Hinzman, L. D., and Kane, D. L.: Spring and aufeis (icing) hydrology in
939 Brooks Range, Alaska, Journal of Geophysical Research: Biogeosciences, 112(G4),
940 10.1029/2006JG000294, 2007.